Transportation Research Part C 158 (2024) 104443

Contents lists available at ScienceDirect

Transportation Research Part C

journal homepage: www.elsevier.com/locate/trc

Infrastructure-Assisted cooperative driving and intersection management in mixed traffic conditions☆

Jun Ying, Yiheng Feng *

Lyles School of Civil Engineering, Purdue University, 550 Stadium Mall Drive, West Lafayette, IN 47907, United States

ARTICLE INFO

Keywords:
Infrastructure-Assisted Cooperative Driving
CAV Trajectory Planning
Traffic Signal Control
Imitation Learning
Integrated Optimization

ABSTRACT

Infrastructure-assisted cooperative driving, which consists of connected and automated vehicle (CAV) trajectory planning and traffic signal control, can greatly improve the efficiency of signalized intersection operations. In existing studies, the CAV trajectory planning problem is simplified to only modeling longitudinal vehicle behaviors or assuming the lane changing can be executed instantaneously. The generated CAV trajectories are not realistic and can't be implemented at the vehicle level. Instantaneous lane changing process may also lead to safety issues or uncomfortable driving behavior of following vehicles in a mixed traffic environment. To fill this research gap, we propose an optimization framework that integrates a full CAV trajectory planning model with traffic signal control in a cooperative driving environment with both CAVs and human-driven vehicles (HDVs). A two-level optimization model is formulated based on discrete time. The high-level model optimizes traffic signal parameters, CAV arrival time, and lane assignment at the stop bar, to minimize total vehicle delay. Given arrival time and lane assignment, the low-level model generates trajectories with integrated car-following and lane-changing maneuvers to mimic a human driving policy based on imitation learning. Numerical experiments from a real-world intersection show that the proposed model outperforms adaptive and fixed time signal control by as much as 63.06% in terms of reduction of average vehicle delay, due to better utilization of lane capacity and reduced lost time. In addition to mobility benefits, fuel consumption is also significantly reduced under the proposed infrastructure-assisted cooperative driving framework.

1. Introduction

Advances in connected and automated vehicle (CAV) technologies are considered to have great potential in improving the efficiency of the transportation system. Through vehicle-to-everything (V2X) communication and/or onboard sensors such as cameras and Lidar, the CAVs can receive and/or capture real-time traffic information from other vehicles and infrastructure to adjust their trajectories to improve safety and reduce delay and fuel consumption. Moreover, the CAVs and infrastructure can be better coordinated through cooperative driving, as illustrated in the Society of Automotive Engineers J3216 standard (Nallamothu et al., 2020). Under the four classes of cooperation, prescriptive is the highest level in which an agent (e.g., an autonomous driving system or an infrastructure own operator (IOO)) has full authority to decide the actions of other road participants and/or infrastructure devices. A typical use case

☆ This article belongs to the Virtual Special Issue on "special issue full title".

* Corresponding author.
E-mail addresses: ying29@purdue.edu (J. Ying), feng333@purdue.edu (Y. Feng).

https://doi.org/10.1016/j.trc.2023.104443
Received 12 March 2023; Received in revised form 3 October 2023; Accepted 27 November 2023

of prescriptive cooperation is the joint optimization of traffic signal timing and CAV trajectories.

In the past few years, this research topic has received wide attention. Li et al. are one of the first researchers that proposed the integrated optimization concept (Li et al., 2014). However, in their work, signal phasing is simplified and is determined by enumeration. Many researchers formulated this problem as a two-level optimization problem, in which the high-level optimizes traffic signal timing and/or vehicle arrival time parameters. The objective function is usually set to minimize vehicle delay or maximize throughput (Islam and Hajbabaie, 2017; Guo et al., 2019). The low-level optimizes vehicle trajectories with energy (or comfort) related objectives such as acceleration fluctuation (Feng et al., 2018) and engine power and brake force (Xu et al., 2019). Yu et al. proposed an integrated optimization model of traffic signals and CAVs' trajectories with a mixed-integer linear programming (MILP) formulation at isolated intersections (Yu et al., 2018) and later at the corridor level (Yu et al., 2019). While most of the earlier works (Li et al., 2014; Yu et al., 2018; Yu et al., 2019) assume that all the vehicles are CAVs (i.e., controllable), recent studies consider a mixed traffic condition with both CAVs and human-driven vehicles (HDVs), such as (Yang et al., 2021; Niroumand et al., 2020; Jiang and Shang, 2022).

No matter considering a full CAV environment or a mixed traffic condition in existing studies, the CAV trajectory planning in the joint control problem is usually simplified in two ways. Some studies only consider longitudinal vehicle control when generating vehicle trajectories and assume the driver needs to take over when lateral maneuvers are required (e.g., mandatory lane changes) (Yang et al., 2021) or assume the vehicles are already generated in the desired lane (Niroumand et al., 2020; Jiang et al., 2021). Other studies model the lane changing maneuver but assume that the lane change can be executed instantaneously (e.g., in one time step) (Yu et al., 2018; Yu et al., 2019). This simplification will result in unrealistic trajectories that violate vehicle dynamics limits and thus can't be executed at the vehicle level. In addition, since the lane changing maneuver also impacts the following vehicle in the target lane, an inaccurate observation/prediction of the lane changing vehicle (e.g., cut-in time) may cause safety issues. Therefore, a full trajectory planning model that includes both continuous longitudinal and lateral vehicle maneuvers is needed.

Trajectory or path planning is an active research topic in autonomous driving. Traditional trajectory or path planning methods can be divided into four categories, including graph search based planning, sampling based planning, interpolating curve-based planning, and optimization based planning (Gonzalez Bautista et al., 2015). Graph search based planning methods traverse states in the grid and give a solution to the path planning problem. Widely used graph search based planning algorithms include Dijkstra algorithm (Anderson et al., 2012; Kala and Warwick, 2013) and A* algorithm (Ferguson et al., 2008). Sampling based planning method (e.g. rapidly-exploring random tree (RRT)) randomly samples the state space and finds connectivity inside it (Elbanhawi and Simic, 2014). For example, (Jeon, et al., 2013) applied RRT for vehicle motion planning by sampling the steering angle. (Kala and Warwick, 2011) adopted RRT to generate trajectories for multiple autonomous vehicles. Interpolating curve-based planning algorithms generate vehicle trajectory by inserting a set of data within the range of previously defined reference points. Clothoid curves (Broggi et al., 2012; Vorobieva et al., 2013), Polynomial curves (Glaser et al., 2010 Sep), or Bezier curves (Zhang et al., 2013) can be applied to generate continuous trajectories for autonomous vehicles. Optimization based planning algorithms generate vehicle trajectory by optimizing parameters such as speed, acceleration, and jerk (Gu and Dolan, 2023; Kogan and Murray, 2006). Recently, with new advances in machine learning techniques, many (deep) reinforcement learning based trajectory planning methods are proposed (Kiran et al., 2021). Other methods that are related to but not the classical reinforcement learning models such as imitation learning also attract increasing attention (Kuderer et al., 2015; Zhang and Cho, 2016). In our previous work (Ying and Feng, 2022), we proposed an imitation learning based full trajectory planning model. Maximum entropy inverse reinforcement learning (IRL) is applied to learn optimal driving policies from demonstrative trajectories. Then the trajectory planning is formulated as an optimization problem with learned optimal driving policy as the objective function with vehicle dynamic constraints. The model generates continuous vehicle trajectories in both longitudinal and lateral dimensions, which essentially integrates the car following and lane changing maneuvers together.

The abovementioned trajectory planning models are usually applied in the context of autonomous driving, where each vehicle makes decisions independently without cooperating with other vehicles and infrastructure. The resultant trajectories may conflict with each other or cannot achieve optimal at the system level in terms of overall efficiency (e.g., total delay). In this paper, we aim to bridge the research gaps by proposing an optimization framework that integrates a full CAV trajectory planning model with traffic signal optimization in a cooperative driving environment. We consider a mixed traffic condition with CAVs and HDVs. We assume that the CAVs are both controllable and observable, while the HDVs are only observable. The observability of HDVs could come from 1) the HDV is a connected vehicle (CV) that broadcasts its real-time status; 2) the HDV's status is captured by infrastructure-based sensors (e.g., cameras); or 3) the HDV's status is captured by nearby CAVs' onboard sensors. The observed HDVs are denoted as observed vehicles (OV) hereafter. Given such a problem, a two-level optimization model is formulated based on discrete time. The high-level model optimizes traffic signal parameters, CAV arrival time at the intersection, and arrival lane assignment, to minimize total vehicle delay and the number of lane changing vehicles. Given arrival time and lane assignment, the low-level model optimizes CAV trajectories and predicts OV future trajectories with integrated car-following and lane changing maneuvers using imitation learning. Specifically, maximum entropy inverse reinforcement learning (IRL), one popular algorithm in imitation learning, is adopted to learn driving behaviors. Training data is collected from historical OV trajectories to make sure the learned CAV driving behaviors are similar to the OVs. Vehicle trajectories are planned or predicted one by one based on their distance to the stop bar. A rolling horizon scheme is applied to incorporate new vehicle arrivals and accommodate OV trajectory perdition errors.

The main contributions of the paper are listed as follows:

1) To the best of our knowledge, this is the first work that integrates a comprehensive and vehicle-level trajectory planning model with traffic signal optimization. The proposed model can generate vehicle trajectories containing both car following and lane changing

Table 1
Variables and notations.

Variables	Meaning
General notations	
i	Arm index
j	Lane index
k	Vehicle index
ϕ	Signal phase index
M	A constant large number
$f()$	Phase lane mapping function
Intersection-level model parameters	
Parameters	
d_{ijk}^{stop}	Distance to stop bar of the k^{th} vehicle in lane j of arm i (m)
ω_{ijk}	The k^{th} vehicle in lane j of arm i
C_i^{NL}	No lane change zone. The area within 70 m to the stop bar.
L_i^{total}	Total lane numbers in arm i
v_l	Vehicle speed limit (m/s^2)
v_{lc}	The lower bound of lane changing vehicle's speed (m/s^2)
v_t	Terminal speed, speed when vehicle passing the intersection (m/s^2)
v_{ijk}	The current speed of the kth vehicle in lane j of arm i (m/s^2)
g_ϕ^p	Green elapse time of phase ϕ (s)
t_ϕ^l	Lost time of phase ϕ (s)
g_{max}	Maximum green duration (s)
g_{min}	Minimum green duration (s)
I_ϕ	Binary parameter. 1 if the current phase is green and 0 otherwise
J_{target}^{ijk}	Target lane group for vehicle ω_{ijk}
v_{ijk}^{lat}	Vehicle ω_{ijk}'s lateral speed (m/s)
d_{ijk}^{lat}	Vehicle ω_{ijk}'s lateral deviation from lane center (m)
f_{ijk}^l	Binary parameter to determine whether a vehicle is making a left lane change. 1 if vehicle ω_{ijk}'s lateral speed is greater than 0 and lateral deviation from the lane center is greater than or equal to 0.2 m and 0 otherwise
f_{ijk}^r	Binary parameter to determine whether a vehicle is making a right lane change. 1 if vehicle ω_{ijk}'s lateral speed is less than 0 and lateral deviation from the lane center is greater than or equal to 0.2 m and 0 otherwise
P_{ijk}	Travel distance from the starting of the lane of the k^{th} vehicle in lane j of arm i (m)
d_{des}	Desire space headway (m)
d_v	Vehicle length (m)
d_g	Minimum space headway from the leading vehicle (m)
$t_{headway}$	Desired time headway (s)
d_r	Desired minimum distance (m)
d_{ijk}^{acc}	Distance vehicle traveled when accelerating from the current speed to speed limit (m)
d_{ijk}^{del}	Distance vehicle traveled when decelerating from the speed limit to terminal speed (m)
v_{avg}^{CAV}	CAV's average speed when close to the intersection (m/s)
v_{avg}^{OV}	OV's average speed when close to the intersection (m/s)
t_{ijk}^{dis}	Time for queue in front of vehicle ω_{ijk} to discharge
I_j^{lm}	Binary parameter. 1 if lane j is the left-most lane and 0 otherwise
I_j^{rm}	Binary parameter. 1 if lane j is the right-most lane and 0 otherwise
d_{max}	Maximum vehicle deceleration in high-level optimization (m/s^2)
a_{max}	Maximum vehicle acceleration in high-level optimization (m/s^2)
I_{safety}	Binary parameter. 1 if the safety distance between vehicle ω_{ijk} and its leading and follow vehicles in the adjacent lane is satisfied and 0 otherwise
I_{speed}	Binary parameter. 1 if the vehicle's current speed is greater than the lower bound when making lane changing and 0 otherwise
I_{NCG}	Binary parameter. 1 if no multiple vehicles change to the same lane in the same gap and 0 otherwise
GAP_j	Set of gaps in lane j
gap_j^q	The q^{th} gap in lane j
d_h	Desire time headway (s)
$K_{front(j)}^{ijk}$	Set of leading vehicles for ego vehicle in lane j
K_L^{qj}	Set of vehicles at the adjacent left lane of gap q in lane j
K_R^{qj}	Set of vehicles at the adjacent right lane of gap q in lane j
d_{dis}	A predefined distance to the stop bar before which the queue is guaranteed to be discharged in the next cycle
$e_{ijk}^{f(j)}$	Binary parameter. 1 if the vehicle enters the intersection when current phase $f(j)$ is red and 0 otherwise
Decision Variables	
d_{ijk}	Delay of the k^{th} vehicle in lane j of arm i (s)
t_{ijk}^a	Arrival time at the stop bar of the k^{th} vehicle in lane j of arm i (s)
r_ϕ	Remaining red time of phase ϕ (s)
g_ϕ	Remaining green duration of phase ϕ (s)

(*continued on next page*)

Table 1 (*continued*)

Variables	Meaning
θ_ϕ	Phase duration (s)
C	Cycle length (s)
δ^0_{ijk}	Binary variable. 1 if the k^{th} vehicle in lane j of arm i will occupy the left-hand side lane in the next time step, and 0 otherwise.
δ^1_{ijk}	Binary variable. 1 if the k^{th} vehicle in lane j of arm i will occupy the current lane in the next time step, and 0 otherwise.
δ^2_{ijk}	Binary variable. 1 if the k^{th} vehicle in lane j of arm i will occupy the right-hand side lane in the next time step, and 0 otherwise.
j_{new}	New lane index of the vehicle after the lane assignment
α_{ijk}	Binary variable. 1 if current phase of lane $jf(j)$ is green and the k^{th} vehicle in lane j of arm i can pass the intersection during the current cycle and 0 otherwise
β_{ijk}	Binary variable. 1 if current phase of lane $jf(j)$ is red and the k^{th} vehicle in lane j of arm i can pass the intersection in the upcoming green duration and 0 otherwise.
t^{dis}_{ijk}	Discharging time for all downstream vehicles of the k^{th} vehicle in lane j of arm i
n^r_{ijk}	Number of downstream vehicles in the adjacent right lane of j_{new} changing to lane j_{new} and joining the queue
n^c_{ijk}	Number of downstream vehicles in the lane of j_{new} maintaining in the queue
n^l_{ijk}	Number of downstream vehicles in the adjacent left lane of j_{new} changing to lane j_{new} and joining the queue
Vehicle-level model parameters	
parameters	
θ	Objective function weight vector
N	Planning horizon
$a_{\max\_L}$	Maximum vehicle acceleration for the vehicle level model (m/s^2)
d_{min}	Minimum safety gap that needs to be satisfied when generating vehicle trajectory
F_{cav}	Binary parameter. 1 if the ego vehicle is CAV, and 0 otherwise
lf_h	Binary parameter. 1 if a leading vehicle exists in the same lane at time step h, and 0 otherwise
m_h	Binary parameter. 1 if a leading vehicle exists in the target lane at time step h, and 0 otherwise
n_h	Binary parameter. 1 if a following vehicle exists in the target lane at time step h, and 0 otherwise
lc	Binary parameter. 1 if the vehicle needs to make a lane change during the planning horizon, and 0 otherwise
ml_h	Binary parameter. 1 if a leading vehicle exists in the left lane at time step h and 0 otherwise
mr_h	Binary parameter. 1 if a leading vehicle exists in the right lane at time step h and 0 otherwise
lc^r	Binary parameter. 1 if the leading vehicle in the left lane changes to the ego vehicle's current lane and 0 otherwise
lc^l	Binary parameter. 1 if the leading vehicle in the right lane changes to the ego vehicle's current lane and 0 otherwise
ψ^r_h	Road heading at time step h
v_{ref}	Reference speed
$\psi_{\max\_rate}$	Maximum heading rate
ψ_{max_diff}	Maximum difference between vehicle heading and road heading
x_{ref}	Reference lateral position
y_{ref}	Reference longitudinal position
$y_{h,front\_adj}$	Target lane leading vehicle longitudinal coordinate at time step h
$y_{h,follow\_adj}$	Target lane following vehicle longitudinal coordinate at time step h
v^{inter}_{min}	Minimum vehicle passing speed at the intersection (m/s^2)
v^{inter}_{max}	Maximum vehicle passing speed at the intersection (m/s^2)
τ	Time gap
Decision variables	
s	Set of vehicle trajectory points
x_h	Vehicle lateral coordinate at time step h
y_h	Vehicle longitudinal coordinate at time step h
v_h	Vehicle speed at time step h (m/s)
a_h	Vehicle acceleration at time step h (m/s^2)
ψ_h	Vehicle heading angle at time step h
$d_{h,des}$	Desire space headway (m)
$d_{h,act}$	Actual space headway (m)

maneuvers (i.e., comprehensive). Trajectories are generated at a high resolution (i.e., 0.1 s) and can be directly applied for vehicle-level execution in real-time.

2) Imitation learning is applied to generate and predict CAV and OV trajectories that can mimic different driving behaviors (accelerate, follow, brake, lane change, etc.). The CAV trajectory generation policy is learned from historical OV trajectories so that they have very similar driving behaviors. The consistent behaviors between the two types of vehicles greatly reduce the heterogeneity in traffic flow, which improves the smoothness and reduces the prediction errors. In addition, the required number of trajectories in the training process is significantly smaller than other deep learning based methods.
3) The proposed framework has great potential to be implemented in a cooperative driving environment with CAVs and connected infrastructure.

The remainder of the paper is arranged as follows. Section II introduces the methodologies including the problem statement, high-level traffic signal and the arrival time/lane assignment optimization, and low-level full trajectory planning model. Section III presents

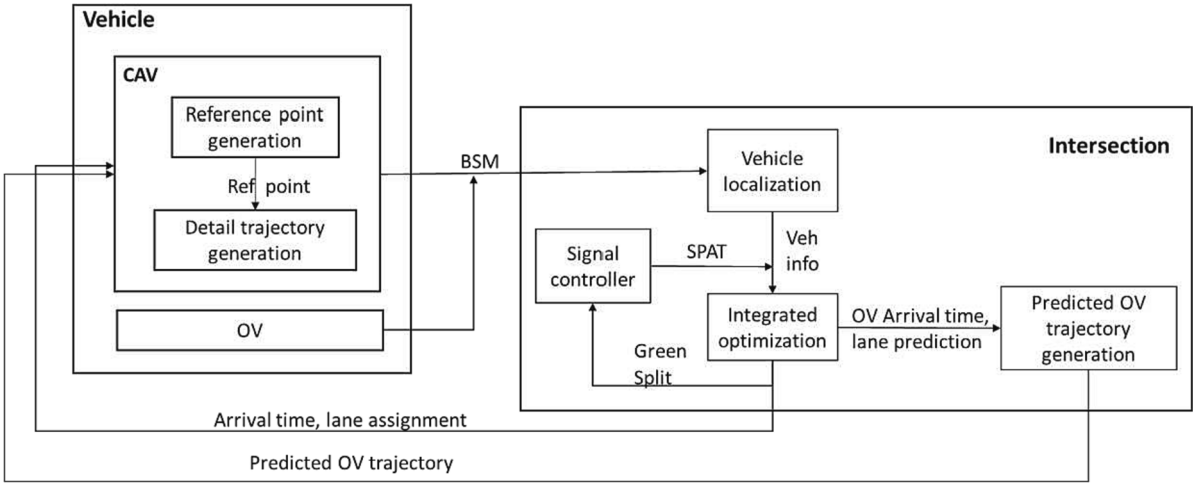

Fig. 1. Optimization model framework.

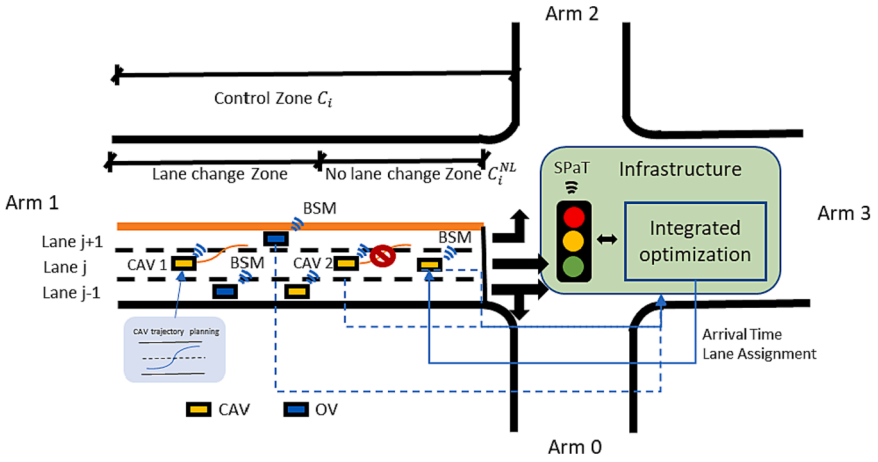

Fig. 2. A typical intersection with four arms.

the solution algorithm for the two-level model and implementation details. Numerical experiments from an isolated intersection are presented in section IV. Section V concludes the work and lays out future research directions.

2. Methodology

2.1. Notations

In this section, parameters and decision variables for the high-level joint optimization model and low-level vehicle trajectory planning model are introduced. Several types of parameters are introduced, including intersection geometric parameters, traffic signal parameters, and vehicle parameters. Intersection geometric parameters mainly describe intersection layout and road heading. Traffic signal parameters include the current green phase, green elapse and remaining time, and lost time. Vehicle parameters denote vehicles' current position and status (speed, acceleration, heading). Decision variables include traffic signal related variables and vehicle related variables. All notations are summarized in Table 1.

2.2. Problem description

In this section, an overview of the optimization framework is provided. The model contains two levels, vehicle level, and intersection level as shown in Fig. 1. We consider a mixed traffic condition with CAVs and OVs. Both CAVs and OVs are observable but only CAVs are controllable. This setting is applied in many previous studies such as (Guo et al., 2019 Jan; Yang et al., 2021 Mar). Through V2X communications, CAVs can broadcast Safety Messages (BSMs) to the intersection. Besides vehicle status information, we also

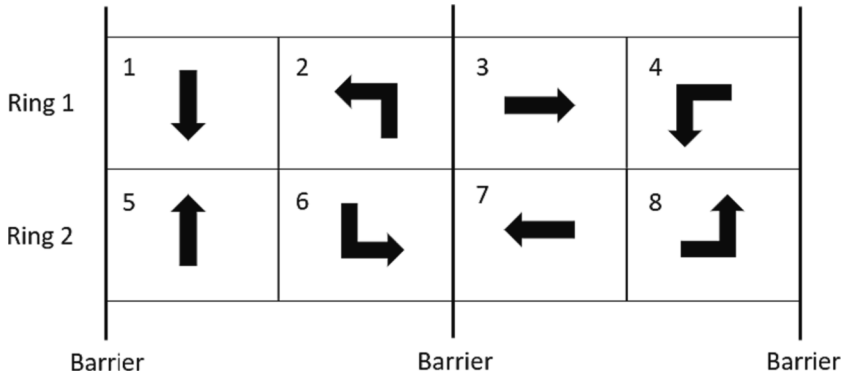

Fig. 3. NEMA dual-ring barrier structure.

assume that CAVs broadcast routing information to the intersection since the intersection needs to assign both arrival travel time and lane index to CAVs, where the assigned lane should be feasible to the vehicle route. As a result, vehicle route is necessary information to provide the feasible lane set based on the intersection channelization. For example, in Fig. 2, a vehicle that travels from west to south (right turning vehicle) should be assigned to the rightmost lane $j+1$. Given BSMs, CAV routes, and signal phasing and timing (SPAT), the intersection controller jointly optimizes the signal timing plan, CAVs' arrival time, and lane assignment at the stop bar. The optimal signal timing plan is sent to the controller to execute. As for the OVs, since they are observed by surrounding CAVs, their status (i.e., in terms of surrogate BSMs) will also be sent to the intersection, but no vehicle routing information. Because the OVs are not controllable, their future trajectories such as arrival time and arrival lane index need to be predicted. In this study, an OV's arrival time is estimated according to its leading and following vehicle arrival time and its position in the queue. An OV's arrival lane index is assumed to be its current lane unless lateral deviation and lateral speed (i.e., a lane changing maneuver) are observed.

OVs' predicted trajectories are generated by the intersection from downstream to upstream and sent to CAVs as surrounding vehicles' future state, along with optimized lane assignment, and arrival time for trajectory generation through the trajectory planning model at the vehicle level. Given the lane assignment and arrival time, each CAV first generates a series of reference points using the trajectory planning model with a large time gap (1 s). Given the reference points, the CAV generates a detailed trajectory with a 0.1 s time gap for vehicle-level execution.

A typical intersection with three types of vehicle movements: left-turning, through, and right-turning is shown in Fig. 2. The arm index starts at zero from the south to north direction, increasing in clockwise order. For each arm, the lane index starts at zero from the right-most lane. Denote C_i as the control zone in arm i. Within the control zone (i.e., communication range), the intersection controller can receive vehicle information and send trajectory planning guidance to CAVs. In this study, we assume the length of the control zone is 300 m, which is a typical V2X communication range. C_i^{NL} is the no lane change zone, which is set to 70 m to the stop bar. Within the no lane change zone, both CAVs and OVs keep their current lanes but the arrival time can still be updated over time. For example, CAV1 can be assigned with both a new lane index and arrival time while CAV2 can only be assigned a new arrival time since it is in the no lane change zone. Next, we will introduce the intersection level (high-level) and vehicle level (low-level) optimization models.

2.3. High-Level optimization model

In this section, the high-level intersection optimization model is presented. The intersection model is responsible for the optimization of traffic signal parameters (green duration and cycle length), CAVs' arrival time, and lane assignments. After entering the intersection control zone, vehicles are mapped to the lane and sorted according to their distance to the stop bar. Vehicle speed and location are obtained from the BSMs, along with the CAV's routing information. Given the vehicle information and SPAT, a mixed integer linear programming (MILP) model is formulated. The main objective of the high-level optimization model is to minimize total vehicle delay with a secondary objective to minimize the number of lane changing CAVs.

$$minimize \sum_i \sum_j \sum_k (d_{ijk} + \delta^0_{ijk} + \delta^2_{ijk}) \tag{1}$$

s.t
signal constraints (eqs (3)–(8)
lane assignment constraints (eqs (9)–(25)
arrival time constraints (eqs (26)–(50)

$$d_{ijk} = t^a_{ijk} - \frac{d^{stop}_{ijk}}{v_l} \tag{2}$$

Where i is the arm index, j is the lane index and k is the vehicle index in the lane. d_{ijk} is the delay of the k^{th} vehicle in lane j, arm i. v_l is the speed limit of the road. d_{ijk} is calculated as the difference between the vehicle arrival time and the free flow travel time. δ^0_{ijk} and δ^2_{ijk} are two binary variables, indicating if the vehicle changes lane to the left/right. Lane change vehicle number is included in the objective function to avoid unnecessary lane changing for CAVs.

2.4. Signal constraints

Signal constraints are formulated based on the NEMA dual-ring barrier structure, as shown in Fig. 3. **Equation (3)** denotes that the summation of the green duration of ring 1 and ring 2 should be equal to the cycle length. **Equations (4) and (5)** illustrate that the green duration of ring 1 and ring 2 should be equal for each barrier. **Equation (6)** demonstrates that when phase ϕ is green, the remaining green duration of phase ϕ is equal to the green duration of phase ϕ subtracting the green elapse time and the lost time. $g_\phi = 0$ when phase ϕ is red. **Equation (7)** denotes that when phase ϕ is red, the remaining red duration of phase ϕ is the summation of the remaining green duration of phase ϕ_g, the time lost in phase ϕ_g and the green duration of phases turning to green before phase ϕ. **Equation (8)** denotes that the green duration of phase ϕ should be bounded by the minimum and maximum green duration.

$$\sum_{i=1}^{4}\theta_{\phi_i} = \sum_{i=5}^{8}\theta_{\phi_i} = C \tag{3}$$

$$\sum_{i=1}^{2}\theta_{\phi_i} = \sum_{i=5}^{6}\theta_{\phi_i} \tag{4}$$

$$\sum_{i=3}^{4}\theta_{\phi_i} = \sum_{i=7}^{8}\theta_{\phi_i} \tag{5}$$

$$g_\phi = I_\phi\left(\theta_\phi - g^p_\phi - t^l_\phi\right), \forall\phi \tag{6}$$

$$r_\phi = (1 - I_\phi)(g_{\phi_g} + t^l_{\phi_g} + \sum_{\phi_p}\theta_{\phi_p}), \forall\phi \tag{7}$$

$$g_{min} \le \theta_\phi \le g_{\max} \tag{8}$$

2.5. Lane assignment constraints

The lane assignment constraints are mainly used to determine whether CAVs need to change lane(s) to reach the next edge on their route or whether the intersection can reduce the total vehicle delay by assigning different lanes. The lane changing behavior of an OV is determined by its own driving model based on the current position and lateral speed, which is assumed to be unknown in the model until certain lateral deviation ($\ge 0.2m$) and speed ($> 0\,m/s$) is observed. OV's arrival time is estimated according to its speed, position, and arrival time of its leading and following vehicle. The details of the constraints are shown in **Equations (9) – (25)**.

$$\sum_{j=0,1,2}\delta^j_{ijk} = 1 \tag{9}$$

$$\delta^{j'}_{ijk} = 0 \text{ if } j' \notin J^{ijk}_{target}, \omega_{ijk} \in \Omega_{CAV} \tag{10}$$

$$f^l_{ijk} = 1 \text{ if } v^{lat}_{ijk} > 0, d^{lat}_{ijk} \ge 0.2 \tag{11}$$

$$f^r_{ijk} = 1 \text{ if } v^{lat}_{ijk} < 0, d^{lat}_{ijk} \le -0.2 \tag{12}$$

$$\delta^1_{ijk} = 1 \text{ if } \omega_{ijk} \in \Omega_{OV}, f^l_{ijk} = 0, f^r_{ijk} = 0 \tag{13}$$

$$\delta^2_{ijk} = 1 \text{ if } \omega_{ijk} \in \Omega_{OV}, f^r_{ijk} = 1 \tag{14}$$

$$\delta^0_{ijk} = 1 \text{ if } \omega_{ijk} \in \Omega_{OV}, f^l_{ijk} = 1 \tag{15}$$

$$j_{new} = \delta^0_{ijk}(j+1) + \delta^1_{ijk}(j) + \delta^2_{ijk}(j-1) \tag{16}$$

Where, δ^j_{ijk} is a binary variable denoting lane occupancy. j' denotes the left-hand side lane, the original lane, and the right-hand side lane. $\delta^0_{ijk} = 1$ if vehicle ω_{ijk} changes to the left-hand side lane, and $\delta^0_{ijk} = 0$ otherwise. Similar for δ^2_{ijk}. $\delta^1_{ijk} = 1$ denotes that vehicle ω_{ijk}

maintains the current lane. Each vehicle can only select the adjacent lane while making a lane change. J^{ijk}_{target} denotes the target lane group for vehicle ω_{ijk}. J^{ijk}_{target} is decided according to vehicle's route. One vehicle may have more than one target lane according to its route. One target lane group has at least one lane and at most L_i^{total} lanes. J^{ijk}_{target} are lanes that have a connection to the next edge on its route. f^l_{ijk} and f^r_{ijk} are binary parameters denoting OV's desire for changing lane to left/right. **Equation (9)** denotes that each vehicle can only change to one lane or occupy the current lane. **Equation (10)** denotes that a CAV should stay within the target lane group or change towards its target lane group. **Equations (11) and (12)** denote the vehicle's desire to change to the left/right-hand side lane. **Equations (13)–(15)** demonstrate OV's lane assignment criteria. An OV will be assigned to its neighboring lane only if it shows a desire for lane changing. **Equation (16)** demonstrates the new lane index according to the vehicle movement.

$$(P_{ij_{new}k^f} - P_{ijk}) - max\left(\frac{v^2_{ijk} - v^2_{ij_{new}k^f}}{2d_{max}} + d_r, d_{des}\right) \geq -\left(1 - \delta^j_{ijk}\right)M \tag{17}$$

$$\left(P_{ijk} - P_{ij_{new}k^{fl}}\right) - max\left(\frac{v^2_{ij_{new}k^{fl}} - v^2_{ijk}}{2d_{max}} + d_r, d_{des}\right) \geq -\left(1 - \delta^j_{ijk}\right)M \tag{18}$$

$$d_r = d_v + d_g \tag{19}$$

$$d_{des} = d_r + t_{headway} \times v_{ijk} \tag{20}$$

$$v_{ijk} - v_{lc} \geq -(1 - \delta^j_{ijk})M \tag{21}$$

$$\delta^1_{ijk} = 1 \text{ if } P_{ijk} \in C_i^{NL} \tag{22}$$

$$\left(1 - I^{lm}_j\right) \sum_{k_l \in K_L^{qj}} \delta^2_{i(j+1)K_L^{qj}} + \left(1 - I^{rm}_j\right) \sum_{k_r \in K_R^{qj}} \delta^0_{i(j-1)K_R^{qj}} \leq 1, \forall gap^q_j \in GAP_J \tag{23}$$

Equations (17)–(19) denote that vehicle ω_{ijk} can move to the adjacent lane only if the safety distance between vehicle ω_{ijk} and the vehicles on the adjacent lane are guaranteed. The safety distance is calculated as the summation of distances that vehicle ω_{ijk} needs to decelerate to the leading vehicle's speed and an extra safety distance. The lower bound of the safety distance is set to the desired space headway, calculated in **Equation (20)**. **Equation (21)** demonstrates that vehicle ω_{ijk} can move to the adjacent lane only when its current speed is larger than v_{lc}. In most of the existing control systems for autonomous vehicles, longitudinal and lateral movement are jointly controlled (Weng et al., 2020). The maximum lateral speed that a vehicle can achieve is constrained by vehicle speed (Definition of Vehicles, Vehicle Types, and Routes - SUMO Documentation [Internet]. [cited, 2023). Low vehicle speed will lead to low lateral speed and a slow lane changing process. Therefore, by setting minimum lane changing speed, **Equation (21)** avoids long lane changing processes, which will lead to potential collisions. **Equations (17)–(21)** are valid when vehicle ω_{ijk} is CAV. **Equation (22)** shows that vehicle ω_{ijk} is supposed to maintain its current lane if it is within the no lane change zone. For a group of vehicles in the same lane, the gap is the space between the leading vehicle and its following vehicle. gap^q_j denotes the q^{th} gap in lane j, index from the downstream to upstream. For any gap^q_j in lane j, at most one vehicle can change to this gap (**Equation (23)**). **Equation (23)** reduces the potential collision by preventing two vehicles from changing lanes towards the same gap.

$$\delta^0_{ijk} = 1, \text{if } j - \min\left(J^{ijk}_{target}\right) < 0, I_{safety} = 1, I_{speed} = 1, I_{NCG} = 1, P_{ijk} \notin C_i^{NL} \tag{24}$$

$$\delta^2_{ijk} = 1, \text{if } j - \max\left(J^{ijk}_{target}\right) > 0, I_{safety} = 1, I_{speed} = 1, I_{NCG} = 1, P_{ijk} \notin C_i^{NL} \tag{25}$$

I_{safety} is a binary parameter indicating whether the safety distance between vehicle ω_{ijk} and its leading and following vehicles in the adjacent lane is guaranteed. $I_{safety} = 1$ denotes that the safety distance is satisfied and 0 otherwise. The calculation of safety distance is the same as **Equations (17)–(20)**. I_{speed} is a binary parameter denoting whether the minimum speed (v_{lc}) for the vehicle to start lane change is satisfied. $I_{speed} = 1$ if the vehicle's current speed is larger than or equal to v_{lc}. $I_{NCG} = 1$ if no vehicles are changing to the same gap according to their route as vehicle ω_{ijk}. $I_{NCG} = 0$ otherwise. For example, two vehicles travel from west to east. The current lane for both vehicles is the leftmost lane and both vehicles need to change to the righthand side lane according to their routes. When the leading and following vehicles in the target lane are the same, two vehicles changing to the same gap may lead to a collision. Therefore, at most one vehicle can utilize the gap. In this case, $I_{NCG} = 0$, the vehicle close to the stop bar will change its lane. $P_{ijk} \notin C_i^{NL}$ demonstrates that vehicle ω_{ijk} is outside the no lane change zone. **Equations (24) and (25)** denote that when vehicle ω_{ijk}'s current lane has no connection to the next edge on its route, vehicle ω_{ijk} can change to the target lane only if the safety distance and initial speed are guaranteed. **Equations (24) and (25)** are valid when vehicle ω_{ijk} is CAV.

2.6. Arrival time constraints

The arrival time constraints determine whether the vehicle can pass through the intersection during the current or next cycle. Assuming the intersection is under-saturated, no vehicle needs to stop twice at the intersection.

$$\phi = f(j) \tag{26}$$

$$M\left(1-\alpha_{ijk}\right) \geq I_{f(j_{new})}\left(t^{a}_{ijk} - g_{f(j_{new})}\right) \geq -M\alpha_{ijk} \tag{27}$$

$$M\alpha_{ijk} \geq I_{f(j_{new})}\left(g_{f(j_{new})} + t^{l}_{f(j_{new})} + C - \theta_{f(j_{new})} + t^{dis}_{ijk} - t^{a}_{ijk}\right) \geq -M(1-\alpha_{ijk}) \tag{28}$$

$$M\beta_{ijk} \geq \left(1 - I_{f(j_{new})}\right)\left(r_{f(j_{new})} + \theta_{f(j_{new})} - t^{a}_{ijk}\right) \geq -M\left(1-\beta_{ijk}\right) \tag{29}$$

$$\left(1 + I_{f(j_{new})}\right) \geq \beta_{ijk} \geq \left(1 - I_{f}(j_{new})\right) \tag{30}$$

$$t^{a}_{ijk} \geq \left(1 - I_{f(j_{new})}\right)\left(r_{f(j_{new})} + t^{dis}_{ijk}\right) \tag{31}$$

$$t^{dis}_{ijk} = \left(n^{r}_{ijk} + n^{c}_{ijk} + n^{l}_{ijk}\right)d_{h} \tag{32}$$

$$n^{r}_{ijk} = n^{r\_green}_{ijk} I_{f(j_{new})} + n^{r\_red}_{ijk}\left(1 - I_{f(j_{new})}\right) \tag{33}$$

$$n^{r\_green}_{ijk} = \sum_{k' \in K^{ijk}_{front(j_{new}-1)}} \left(1 - \alpha_{i(j_{new}-1)k'}\right)\left(\delta^{0}_{i(j_{new}-1)k'}\right) \tag{34}$$

$$n^{r\_red}_{ijk} = \sum_{k' \in K^{ijk}_{front(j_{new}-1)}} \left(\beta_{i(j_{new}-1)k'}\right)\left(\delta^{0}_{i(j_{new}-1)k'}\right) \tag{35}$$

$$n^{c}_{ijk} = n^{c\_green}_{ijk} I_{f(j_{new})} + n^{c\_red}_{ijk}\left(1 - I_{f(j_{new})}\right) \tag{36}$$

$$n^{c\_green}_{ijk} = \sum_{k' \in K^{ijk}_{front(j_{new})}} \left(1 - \alpha_{ij_{new}k'}\right)\left(\delta^{1}_{ij_{new}k'}\right) \tag{37}$$

$$n^{c\_red}_{ijk} = \sum_{k' \in K^{ijk}_{front(j_{new})}} \left(\beta_{ij_{new}k}\right)\left(\delta^{1}_{ij_{new}k}\right) \tag{38}$$

$$n^{l}_{ijk} = n^{l\_green}_{ijk} I_{f(j_{new})} + n^{l\_red}_{ijk}\left(1 - I_{f(j_{new})}\right) \tag{39}$$

$$n^{l\_green}_{ijk} = \sum_{k' \in K^{ijk}_{front(j_{new}+1)}} \left(1 - \alpha_{i(j_{new}+1)k'}\right)\left(\delta^{2}_{(j_{new}+1)k'}\right) \tag{40}$$

$$n^{l\_red}_{ijk} \sum_{k' \in K^{ijk}_{front(j_{new}+1)}} \left(\beta_{i(j_{new}+1)k'}\right)\left(\delta^{2}_{i(j_{new}+1)k'}\right) \tag{41}$$

Where $f(\bullet)$ is the function that maps the lane to phases. **Equations (27) and (28)** are valid when the current phase $f(j_{new})$ is green. **Equation (27)** denotes that if vehicle ω_{ijk} passes the intersection during the current cycle, the vehicle arrival time should be less than the remaining green duration. **Equation (28)** demonstrates that if the vehicle ω_{ijk} passes the intersection during the next cycle, the vehicle arrival time should be larger than the summation of the remaining green duration of phase $f(j_{new})$, the lost time of phase $f(j_{new})$, the time before phase $f(j_{new})$ turns to green in the next cycle and the queue discharge time in the lane j_{new}. **Equations (29) and (31)** are valid when the current phase $f(j_{new})$ is red. **Equation (29)** demonstrates that if vehicle ω_{ijk}'s arrival time is less than the summation of the remaining red duration and the green duration of phase $f(j_{new})$, the vehicle will pass through the intersection when phase $f(j_{new})$ turns green in the current cycle. **Equation (30)** denotes that vehicle ω_{ijk}arrives at the intersection when the phase $f(j_{new})$ is red will pass through the intersection when phase $f(j_{new})$ turns green. **Equation (30)** avoids the vehicle stopping twice at the intersection. **Equation (31)** demonstrates that if vehicle ω_{ijk} arrives at the intersection when phase $f(j_{new})$ is red, its arrival time should be greater than the summation of the remaining red duration of phase $f(j_{new})$ and the discharging time of its leading vehicle. **Equation (32)** denotes the

time for the queue in front of vehicle ω_{ijk} to discharge. **Equation (33)** calculates the number of leading vehicles in the adjacent right lane of j_{new} changing to lane j_{new} and waiting in the queue, considering the status of the current phase $f(j_{new})$. When the current phase $f(j_{new})$ is green and vehicle ω_{ijk} can't pass the intersection during the current green phase, $n_{ijk}^{r\_green}$ is equal to the number of leading vehicles in the adjacent right lane of j_{new} changing to lane j_{new} but can't pass the intersection in the current cycle, as shown in **Equation (34)**. **Equation (35)** is valid when the current phase $f(j_{new})$ is red, and $n_{ijk}^{r\_red}$ is equal to the number of leading vehicles in the adjacent right lane of j_{new} changing to lane j_{new}. **Equations (36)–(38)** calculate the number of leading vehicles in the lane j_{new} maintaining in j_{new} and waiting in the queue. **Equations (39)–(41)** calculate the number of leading vehicles in the adjacent left lane of j_{new} changing to lane j_{new} and wait in the queue.

$$t_{ijk}^{a} \geq \frac{d_{ijk}^{stop} - d_{ijk}^{acc} - d_{ijk}^{dec}}{v_l} + \frac{v_l - v_{ijk}}{a_{max}} + \frac{v_l - v_t}{d_{max}} \text{ if } d_{ijk}^{stop} \geq d_{ijk}^{acc} + d_{ijk}^{dec} \tag{42}$$

$$t_{ijk}^{a} \geq \frac{d_{ijk}^{stop}}{v_{avg}^{CAV}} \text{ if } \omega_{ijk} \in \Omega_{CAV}, d_{ijk}^{stop} < d_{ijk}^{acc} + d_{ijk}^{dec} \tag{43}$$

$$t_{ijk}^{a} \geq \frac{d_{ijk}^{stop}}{v_{avg}^{OV}} \text{ if } \omega_{ijk} \in \Omega_{OV}, d_{ijk}^{stop} < d_{ijk}^{acc} + d_{ijk}^{dec}, v_{ijk} \leq v_{avg}^{OV} \tag{44}$$

$$t_{ijk}^{a} \geq \frac{d_{ijk}^{stop}}{v_{ijk}} \text{ if } \omega_{ijk} \in \Omega_{OV}, d_{ijk}^{stop} < d_{ijk}^{acc} + d_{ijk}^{dec}, v_{ijk} > v_{avg}^{OV} \tag{45}$$

$$t_{ijk}^{a} \geq (r_{f(j_{new})} + t_{ijk}^{dis})(1 - I_{f(j_{new})}) \tag{46}$$

$$t_{ijk}^{a} \geq (t_{ij_{new}k'} + d_h)\delta_{ij_{new}k'}^{1}, k' \in \boldsymbol{K}_{\boldsymbol{front}(\boldsymbol{j_{new}})}^{\boldsymbol{ijk}} \tag{47}$$

$$t_{ijk}^{a} \geq (t_{i(j_{new}-1)k'} + d_h)\delta_{ij_{new}k'}^{0}, k' \in \boldsymbol{K}_{\boldsymbol{front}(\boldsymbol{j_{new}}-1)}^{\boldsymbol{ijk}} \tag{48}$$

$$t_{ijk}^{a} \geq (t_{i(j_{new}+1)k'} + d_h)\delta_{ij_{new}k'}^{2}, k' \in \boldsymbol{K}_{\boldsymbol{front}(\boldsymbol{j_{new}}+1)}^{\boldsymbol{ijk}} \tag{49}$$

$$\alpha_{ijk} = 1 \text{if } d_{ijk}^{stop} \leq d_{dis} \text{ and } e_{ijk}^{f(j)} = 1 \tag{50}$$

Equation (42) denotes that vehicle ω_{ijk}'s arrival time is larger than the summation of the time that the vehicle accelerates to the speed limit, decelerates to the terminal speed v_t and travel with the free flow speed between the two processes. **Equation (42)** is valid when vehicle's distance to the stop bar is larger than the summation of vehicle's acceleration and deceleration distance. **Equation (43)** limits CAV's arrival time to be larger than the time that the vehicle travels to the stop bar with average speed when approaching the intersection. **Equations (44) and (45)** constrain OV's arrival time, which depends on OV's average speed when approaching the intersection and current speed v_{ijk}. **Equations (43)–(45)** are valid when vehicle's distance to the stop bar is not enough for the accelerate and decelerate process. **Equation (46)** constrains vehicle ω_{ijk}'s arrival time to be larger than the summation of the remaining red duration and the time for the queue in front of the ego vehicle to discharge. **Equation (47)** shows that vehicle ω_{ijk}'s arrival time should be greater than the immediate leading vehicle arrival time in the lane j_{new} that maintains its current lane plus a constant time headway. **Equations (48) and (49)** show that vehicle ω_{ijk}'s arrival time should be greater than the leading vehicle's arrival time in the adjacent right/left lane of the lane j_{new} but changing to lane j_{new} plus the constant time headway. **Equation (50)** guarantees that the queue before d_{dis} (e.g., 100 m in this study) from the stop bar will be discharged in the next cycle. $e_{ijk}^{f(j)} = 1$ denotes that the vehicle enters the intersection when the current phase $f(j)$ is red. **Equation (50)** avoids the queue building up in directions with uneven vehicle distribution.

2.7. Low-Level trajectory planning model

In this section, the low-level vehicle trajectory planning model is introduced. Given the lane assignment and arrival time from the high-level optimization model, each CAV generates its own trajectory using the trajectory planning model. The same trajectory planning model is applied to predict OV's movement and used as a reference when generating CAVs' trajectories. The trajectory planning model is formulated as a nonlinear optimization problem and is shown in **Equation (51)**. $\boldsymbol{\theta}^T f(\boldsymbol{s}, \boldsymbol{u})$ is the cost function, $\boldsymbol{\theta}$ is the weight vector, and is learned using maximum entropy inverse reinforcement learning (IRL) (Ying and Feng, 2022). $\boldsymbol{s} = (s_1, s_2, \cdots, s_N)$. N is the planning horizon. s_h denotes the trajectory point at time step h. Each trajectory point s_h is a combination of x_h; y_h, v_h, a_h, ψ_h. x_h and y_h are the lateral and longitudinal coordinates at time step h. v_h denotes the vehicle speed. a_h denotes the vehicle acceleration. ψ_h is the vehicle's heading angle at time step h. $\boldsymbol{u}$ denotes vehicle's initial state, environmental parameters, and input from the high-level optimization. Vehicle initial states include vehicle's position and vehicle status (acceleration, speed, and heading angle). Environment parameters include the surrounding vehicles' positions and status (acceleration, speed) over the planning horizon and road geometry

information (speed limit, lane heading). Objective function feature selection and constraints will be introduced in the following section. More details on how to use IRL to obtain the optimal weight vector can be found in our previous study (Ying and Feng, 2022).

$$minimize_s \boldsymbol{\theta}^T f(\boldsymbol{s}, \boldsymbol{u}) \tag{51}$$

s.t
vehicle dynamics constraints (eqs (63)–(70)
safety constraints (eqs (71)–(75)
Cost function

The cost function is a linear combination of representative driving features. 11 features are selected in total, concerning safety, comfort, and consistency with high-level guidance. The proposed features are generic and can be applied to different driving scenarios, including free flow, car following, and lane changing. Lane assignment from the high-level guidance is converted to a reference position in the cost function. If the initial lane and the lane assignment are the same, a car-following trajectory will be generated. Otherwise, a lane changing trajectory will be generated. Arrival time is converted to the planning horizon (N). Given the initial state and the high-level guidance, the generated trajectory can guide the vehicle to arrive at the reference point at the end of the planning horizon. Next, the selected features in the cost function are introduced.

$$f_1 = \frac{1}{N}\sum_{h=1}^{N} a_h^2 \tag{52}$$

$$f_2 = \frac{1}{N-1}\sum_{h=1}^{N-1} (a_{h+1} - a_h)^2 \tag{53}$$

$$f_3 = \frac{1}{N-1}\sum_{h=1}^{N-1} (\psi_{h+1} - \psi_h)^2 \tag{54}$$

Equation (52) denotes the average square of acceleration fluctuation a_h^2. **Equation (53)** denotes the average square of jerk for the whole trajectory. **Equation (54)** measures the vehicle heading change rate. **Equations (52)–(54)** punish the uncomfortable motions (large acceleration or vehicle heading change) and keep the trajectory smooth and comfortable.

$$f_4 = \frac{1}{N}\sum_{h=1}^{N} (d_{h,des} - d_{h,act})^2 lf_h = \frac{1}{N}\sum_{h=1}^{N} \left(d_{min} + t_{headway} v_h - d_{h,act}\right)^2 lf_h \tag{55}$$

$$f_5 = \frac{1}{N}\sum_{h=1}^{N} \frac{1}{\left(\alpha + y_{h,front_{adj}} - y_h\right)^2} m_h lc_h \tag{56}$$

$$f_6 = \frac{1}{N}\sum_{h=1}^{N} \frac{1}{\left(\alpha + y_h - y_{h,follow_{adj}}\right)^2} n_h lc_h \tag{57}$$

$$f_7 = \frac{1}{N}\sum_{h=1}^{N} \left(\psi_h - \psi_h^r\right)^2 \tag{58}$$

Equations (55)–(58) are safety-related features. **Equation (55)** measures the difference between the desired space headway and the actual space headway. α is a constant to avoid f_5,f_6 becoming too large. **Equations (56) and (57)** guarantee vehicle safety by maximizing the distance between the ego vehicle and the leading/following vehicle in the target lane. ψ_h^r is the road heading. **Equation (58)** limits the vehicle from deviating from the road.

$$f_8 = \left(x_N - x_{ref}\right)^2 \tag{59}$$

$$f_9 = \left(y_N - y_{ref}\right)^2 \tag{60}$$

$$f_{10} = \frac{1}{N}\sum_{h=1}^{N} \left(x_h - x_{ref}\right)^2 \tag{61}$$

$$f_{11} = \frac{1}{N}\sum_{h=1}^{N} \left(y_h - y_{ref}\right)^2 \tag{62}$$

Equations (59) and (60) measure the difference between the vehicle's terminal position and the reference position. f_8 and f_9 guarantee the consistency between the low-level trajectory planning model and the high-level optimization model. f_8 and f_9 also guarantee the vehicle reaches the stop bar and assigned lane at the end of the planning horizon. **Equations (61) and (62)** push the vehicle to reach the stop bar and assigned lane as soon as possible. **Equations (61) and (62)** avoid the lane changing process being too long,

which may lead to a potential collision with other vehicles.

2.8. Vehicle dynamic constraints

In this section, vehicle dynamic constraints are introduced. **Equations (63)–(70)** demonstrate vehicle kinematic motion and vehicle kinematic parameter boundaries, which are valid for both CAVs and OVs. **Equations (63)–(65)** denote vehicle kinematic motions. **Equations (66)–(70)** demonstrate vehicle kinematic parameters' boundaries. **Equation (66)** limits the vehicle acceleration and deceleration. **Equation (67)** denotes the vehicle heading change rate constraints. **Equation (68)** limits the difference between vehicle heading and road heading. **Equation (69)** limits vehicle's maximum speed. **Equation (70)** limits vehicle speed when passing the intersection. **Equation (70)** is valid only if the ego vehicle is a CAV and its terminal position is the stop bar.

$$x(t+1) = x(t) + (v\tau + \frac{1}{2}a\tau^2)cos(\psi(t)) \tag{63}$$

$$y(t+1) = y(t) + (v\tau + \frac{1}{2}a\tau^2)sin(\psi(t)) \tag{64}$$

$$v(t+1) = v(t) + \tau a(t) \tag{65}$$

$$-a_{\max\_L} \le a(t) \le a_{\max\_L} \tag{66}$$

$$-\psi_{m\_rate} \le \frac{\psi(t+1) - \psi(t)}{\tau} \le \psi_{\mathrm{m}\_rate} \tag{67}$$

$$-\psi_{\max\_diff} \le \psi(t) - \psi^r(t) \le \psi_{\max\_diff} \tag{68}$$

$$v(t) \le v_l \tag{69}$$

$$v_{min}^{inter} \le v(N) \le v_{max}^{inter} \tag{70}$$

2.9. Vehicle safety constraints

Vehicle safety constraints are demonstrated in this section. F_{CAV} is a binary parameter indicating whether the ego vehicle is CAV. $F_{CAV} = 1$ is the ego vehicle is CAV and 0 otherwise. **Equations (71)–(73)** guarantee the safety distance between the ego vehicle and the surrounding vehicles (leading vehicle in the same lane, leading and following vehicles in the target lane). Safety distance is calculated as the summation of distances the vehicle needs to decelerate to the leading vehicle speed and an additional safety gap d_r. If the ego vehicle's current speed is less than its leading vehicle's speed, the safety distance is considered as d_r. For OV, the safety distance is considered d_r. **Equation (71)** is valid when the leading vehicle in the same lane exists. **Equations (72) and (73)** are valid when the ego vehicle changes its lane during the planning horizon and the leading/following vehicle in the target lane exists.

$$\left(y_{i,front} - y_i\right) \ge max\left(\frac{v_i^2 - v_{i,front}^2}{2a_{max\_L}}, 0\right) \times F_{CAV} + d_r \text{ if } lf_i = 1 \tag{71}$$

$$\left(y_{i,front\_adj} - y_i\right) \ge max\left(\frac{v_i^2 - v_{i,front_{adj}}^2}{2a_{max\_L}}, 0\right) \times F_{CAV} + d_r \text{ if } m_i lc_i = 1 \tag{72}$$

$$\left(y_i - y_{i,follow\_adj}\right) \ge max\left(\frac{v_{i,follow_{adj}}^2 - v_i^2}{2a_{max\_L}}, 0\right) \times F_{CAV} + d_r \text{ if } n_i lc_i = 1 \tag{73}$$

Equations (74) and (75) enable the cooperative lane changing and guarantee the safety distance between the ego vehicle and the left/right leading vehicle changing lane to the current lane during the whole lane change process. **Equations (74) and (75)** are valid when the ego vehicle is CAV and the leading vehicle in the neighboring lane exists and will change lane to the current lane according to high-level lane assignment. A CAV cooperates with its leading lane changing vehicle by taking the leading vehicle state as a reference and generating its own trajectory, potentially reducing the collision probability, and guaranteeing the safety gap during the lane change process.

$$\left(y_{i,front\_l} - y_i\right) \ge \max\left(\frac{v_i^2 - v_{i,front_l}^2}{2a_{\max\_L}}, 0\right) + d_r \text{ if } mr_i lc_i^r = 1 \tag{74}$$

$$\left(y_{i,front\_r} - y_i\right) \ge \max\left(\frac{v_i^2 - v_{i,front_r}^2}{2a_{\max\_L}}, 0\right) + d_r \text{ if } ml_i lc_i^l = 1 \tag{75}$$

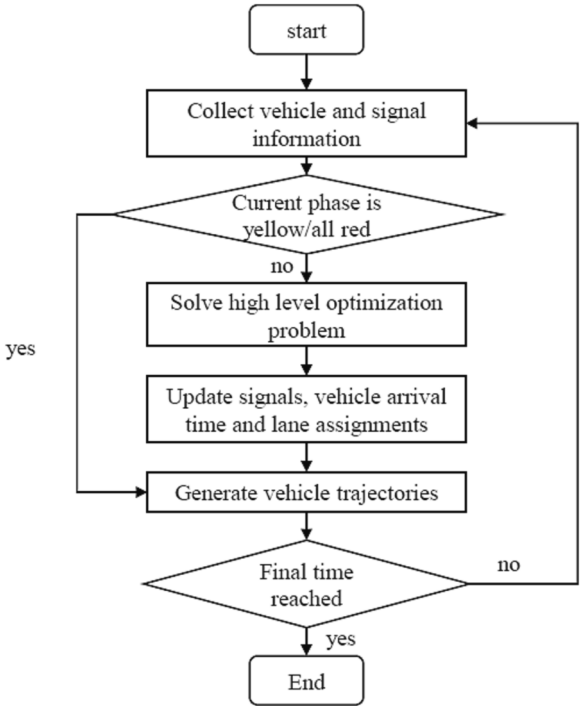

Fig. 4. Implementation framework.

Equations (63)−(69), (71)−(73) are valid for both CAV and OV. **Equations (70),(74),(75)** are valid only when the ego vehicle is CAV.

3. Solution algorithms

3.1. Model implementation

The implementation of the two-level optimization framework is described in this section. A flow chart of the implementation procedure is shown in Fig. 4. Vehicle and signal information are collected at the beginning of every time step. If the traffic signal status is not in the transition period (yellow or all-red), the high-level optimization problem is solved to generate the optimal signal timing plan, CAV arrival time, CAV lane assignments, and predicted OV arrival time. CAV arrival time and lane assignments are sent to CAVs, and each CAV generates its detailed trajectory. If the signal status is in the transition period, signal timing will remain the same. CAVs generate their trajectories according to the previously allocated lane index and arrival time. A rolling horizon scheme is applied at the high-level optimization model to include new vehicle arrivals. The signal timing plan is generated for one cycle, but only the first second is implemented. A similar rolling horizon scheme is applied to the vehicle level trajectory generation, where only the first second of the generated trajectory is implemented. Vehicle arrival time and lane assignment are also updated every second, except when the signal status is in the transition period.

3.2. Trajectory generation procedure

Given the vehicle arrival time and lane assignment from the high-level model, details of the trajectory generation procedure for both CAVs and OVs are described in the following steps and shown in Fig. 5.

Step 1: Receive vehicle arrival time and lane assignment from the high-level model.
Step 2: Determine whether reference points need to be generated. If vehicle arrival time is greater than 6 s, then reference points will be generated in **Step 3**. Otherwise, detailed trajectories will be generated in **Step 5**.
Step 3: Generate reference trajectory points by solving the low-level trajectory generation model with time step (τ) equal to 1 s, the terminal position at the stop bar, and the planning horizon equal to the arrival time.
Step 4: If the solution is feasible, go to **Step 5**. Otherwise, the vehicle will execute a car-following model. In this study, the Intelligent Driving Model(IDM) is used.
Step 5: Solve the low-level trajectory generation model with $\tau = 0.1s$. The maximum planning horizon for the low-level trajectory generation model is set to 6 s to guarantee sufficient lane change time. If the vehicle arrival time is greater than 6 s, the terminal

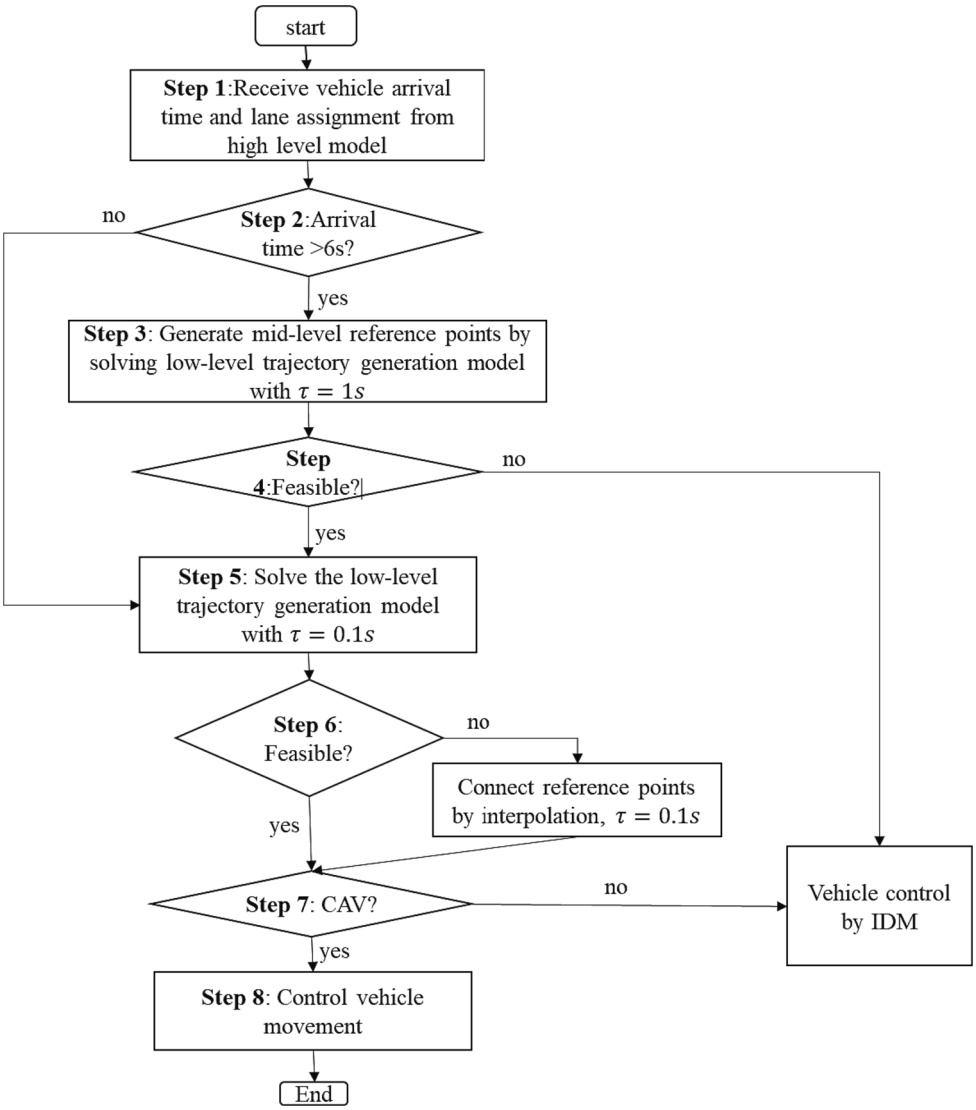

Fig. 5. Trajectory generation procedure.

point is set to the reference point at $t = 6s$ and the planning horizon is set to 6 s. Otherwise, the terminal position is set at the stop bar and the planning horizon is set to vehicle's arrival time.

Step 6: If the model is feasible, go to **Step 7**. Otherwise, connect the generated reference points from **Step 3** by interpolation with $\tau = 0.1s$.

Step 7: If the vehicle is a CAV, go to **Step 8**. Otherwise, the vehicle executes a car-following model.

Step 8: Control vehicle movement.

According to the high-level intersection optimization model, vehicles assigned to pass the intersection during the next cycle or when arriving on red may have longer arrival time (e.g., >30 s). The solving time of the trajectory generation model increases dramatically when the planning horizon is long. For example, the average solving time with the planning horizon equals 6 s is less than 0.1 s but quickly increases to 1 s when the planning horizon is around 30 s. Besides, vehicle state and assigned arrival time vary at each time step. Generating detailed trajectory for the entire planning horizon is inaccurate and unnecessary. As a result, we divide the planning horizon into small segments (6 s in our case) when it is too long. In addition, solving the low-level model for the first 6 s without considering the terminal condition will lead to infeasible solutions when the vehicles are too close to the intersection. In order to guarantee feasible solutions for all segments of short planning horizon, as well as improve the solving time, mid-level reference points are generated with time gap $\tau = 1\,s$, which essentially provides terminal points for each short segment. For rare cases, the optimization can't generate feasible solutions, vehicles will be controlled by a car-following model (i.e., IDM). Vehicle trajectories are generated in sequence based on their distance to the stop bar. Upstream CAVs can utilize downstream vehicles' planned trajectories

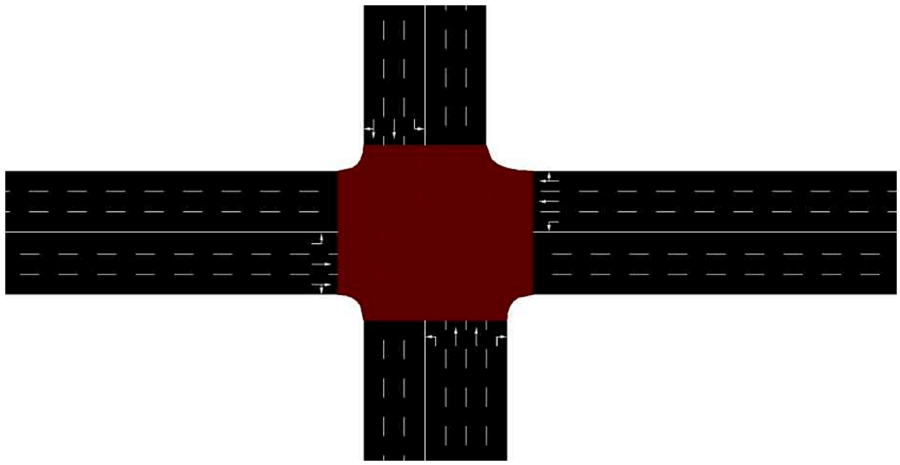

Fig. 6. Plymouth Rd. and Huron Pkwy.

Table 2
Traffic volume (veh/h).

	Left turn	Through movement	Right turn
Westbound	205	773	109
Eastbound	12	826	179
Northbound	251	308	338
Southbound	192	227	13

Table 3
Simulation parameters.

Parameter name	Value
Speed limit	16.7 m/s
Minimum green time	6 s
Maximum green time	100 s
Yellow interval	3 s
All-red clearance interval	1 s
CAV headway	1.8 s
OV headway	1.6 s, 1.8 s, 2.0 s
Maximum acceleration (intersection level)	5 m/s^2
Maximum deceleration (intersection level)	5 m/s^2
Maximum acceleration (vehicle level)	9 m/s^2
Maximum vehicle heading change rate	$\pi/4$
Maximum deviation from road heading	$\pi/6$
Vehicle length	5 m
Desired safety distance	8 m
Desired safety gap with front vehicle	3 m
Minimum safety distance	7.3 m
Minimum speed vehicle start lane changing	6m/s
Maximum planning horizon (low level)	6 s

(CAVs) or predicted trajectories (OVs) when generating their own trajectories.

4. Numerical experiments

To validate the proposed model and ensure the simulation results are meaningful, a real-world intersection (Plymouth Rd and Huron Pkwy) in Ann Arbor, Michigan is built in SUMO, as shown in Fig. 6. The control zone is set to 300 m. The no lane change zone in each arm is set to 70 m. The volumes and turning ratios of each movement are calibrated with the real traffic demand collected from the afternoon peak hour (4:00p.m. – 5:00p.m.), as shown in Table 2**.** The CAV penetration rates are set to 25 %, 50 %, 75 %, and 100 %. The desired speeds (v_{min}^{inter}, v_{max}^{inter}) for vehicles passing the intersection are 8–10 m/s. To incorporate the uncertainties in OV's car-following behavior, the desired time headway for HDV is set to be three different values, 1.6 s, 1.8 s, and 2.0 s. Other simulation parameters are summarized in Table 3.

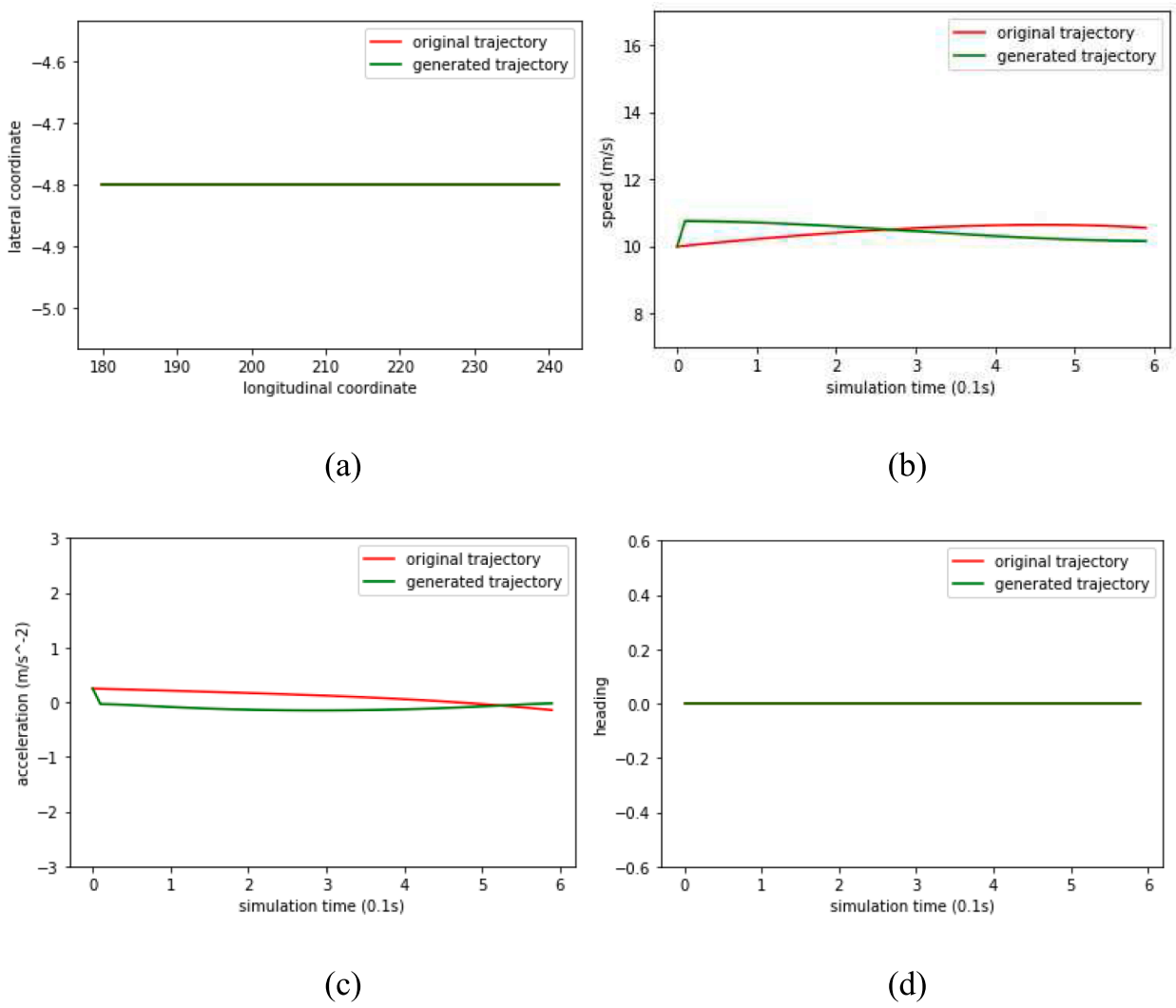

Fig. 7. Comparison between Ground Truth and Generated Trajectory (Car-following).

The optimization model is solved using Gurobi (Leader, 2023) at the high-level and Pyomo (Pyomo [Internet]. Pyomo. [cited, 2023) at the low-level. The high-level intersection optimization model can be solved within 0.1 s with a 0.1 % gap to the optimal solution. For the low-level trajectory planning model, the optimal solution can also be found within 0.1 s, which guarantees real-time performance.

Two baselines are set up for comparison 1) fixed time control without trajectory optimization; and 2) adaptive signal control without trajectory optimization. The fixed time control is generated according to Webster's optimal cycle length model (Mannering and Washburn, 2020). The formulation of the adaptive signal control model is the same as the proposed high-level model with 0 % CAV penetration rate (i.e., all vehicles are OVs). Vehicle arrival time and lane assignment are generated but are not sent to vehicles. All the vehicles are controlled by SUMO internal models, where the intelligent driving model (IDM) (SUMO Documentation, 2023) is used for car-following model with driver reaction time set to 1.6 s, 1.8 s, and 2.0 s. SUMO's internal sub-lane model "SL2015" (SUMO Documentation, 2023) is selected as the lane changing model with lateral resolution equal to 0.1 s. Other parameters such as the rolling horizon settings and signal lost time remain the same. In the low-level trajectory planning model, weight vectors for the selected features are obtained by IRL. To avoid redundancy, more details of the training process and validation can be found in our previous study (Ying and Feng, 2022). The total simulation time for each scenario is 1800 s, with the simulation step size equal to 0.1 s. To make a fair comparison, the mean desired headway for both SUMO-controlled vehicles in the baselines and CAVs in the proposed model is set to be equal to 1.8 s.

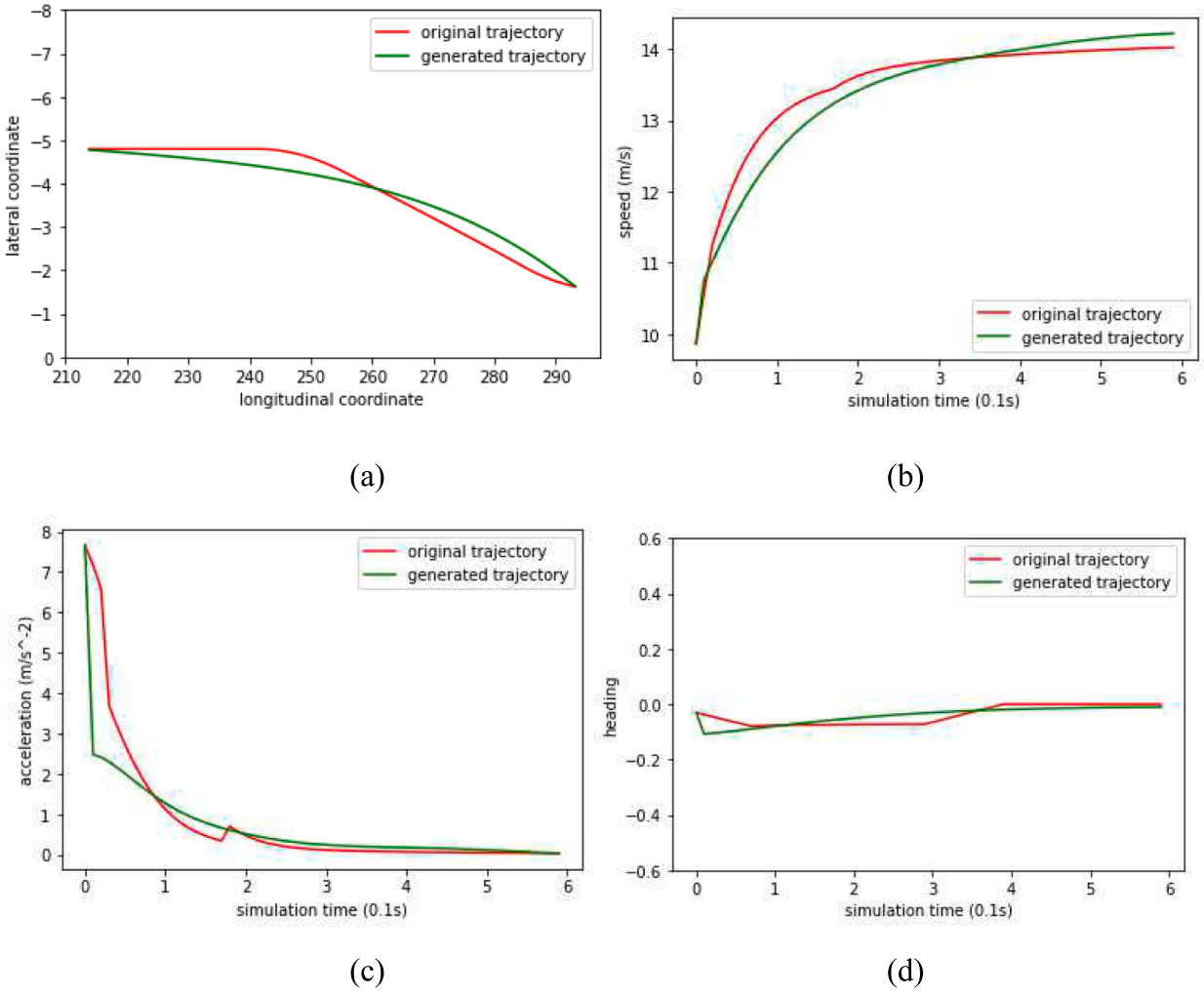

Fig. 8. Comparison between Ground Truth and Generated Trajectory (Lane Changing).

4.1. Trajectory planning model evaluation

To train the IRL model, 119 SUMO-controlled vehicle trajectories are extracted from simulation. 25 trajectories are used for training and 94 trajectories are used for testing. In both training and testing datasets, 52 % of the trajectories are car-following scenarios and 48 % conduct lane-changing maneuvers. The resolution of the trajectory is 0.1 s, which is the same as the trajectory planning resolution. The length of the trajectory is 6 s, which is the same as the low-level model's maximum planning horizon.

Fig. 7 shows the comparison between the generated trajectory and the ground truth trajectory for the car following scenario. In Fig. 7**(a)**, the x-axis is the longitudinal coordinate, and the y-axis is the lateral coordinate. As shown in Fig. 7**(a)**, the generated trajectory has a similar position profile as the ground truth trajectory. Since there is no lateral deviation, the generated trajectory overlaps with the ground truth trajectory. Fig. 7**(b)(c)(d)** show the speed, acceleration, and vehicle heading angle profiles. The generated trajectory has a very similar trend as the ground truth trajectory in all profiles.

Fig. 8 shows an example of comparison between the generated trajectory and the ground truth trajectory under lane changing scenario. The figure shows that the generated trajectory has a similar profile as the ground truth trajectory, in terms of position, speed, acceleration, and heading angle.

To further evaluate the accuracy of the trajectory planning model, average displacement error (ADE) and final displacement error (FDE) are used to measure the difference between the generated trajectory and the ground truth trajectory, as shown in **Equations (76) and (77)**. (x_i^g, y_i^g) denotes the coordinate of the generated trajectory at time step *i*. (x_i^o, y_i^o) denotes the coordinate of ground truth trajectory at time step *i*. *N* is the total length of the trajectory.

$$ADE = \frac{\sum_{i=1}^{N} \sqrt{(x_i^g - x_i^o)^2 + (y_i^g - y_i^o)^2}}{N} \tag{76}$$

Table 4
ADE and FDE of the Trajectory Generation Model.

	ADE	FDE	ADE (lateral)	ADE (longitudinal)
In-lane	0.90	0.01	0.00	0.90
Lane changing	1.68	0.12	0.27	1.61
All	1.27	0.06	0.13	1.24

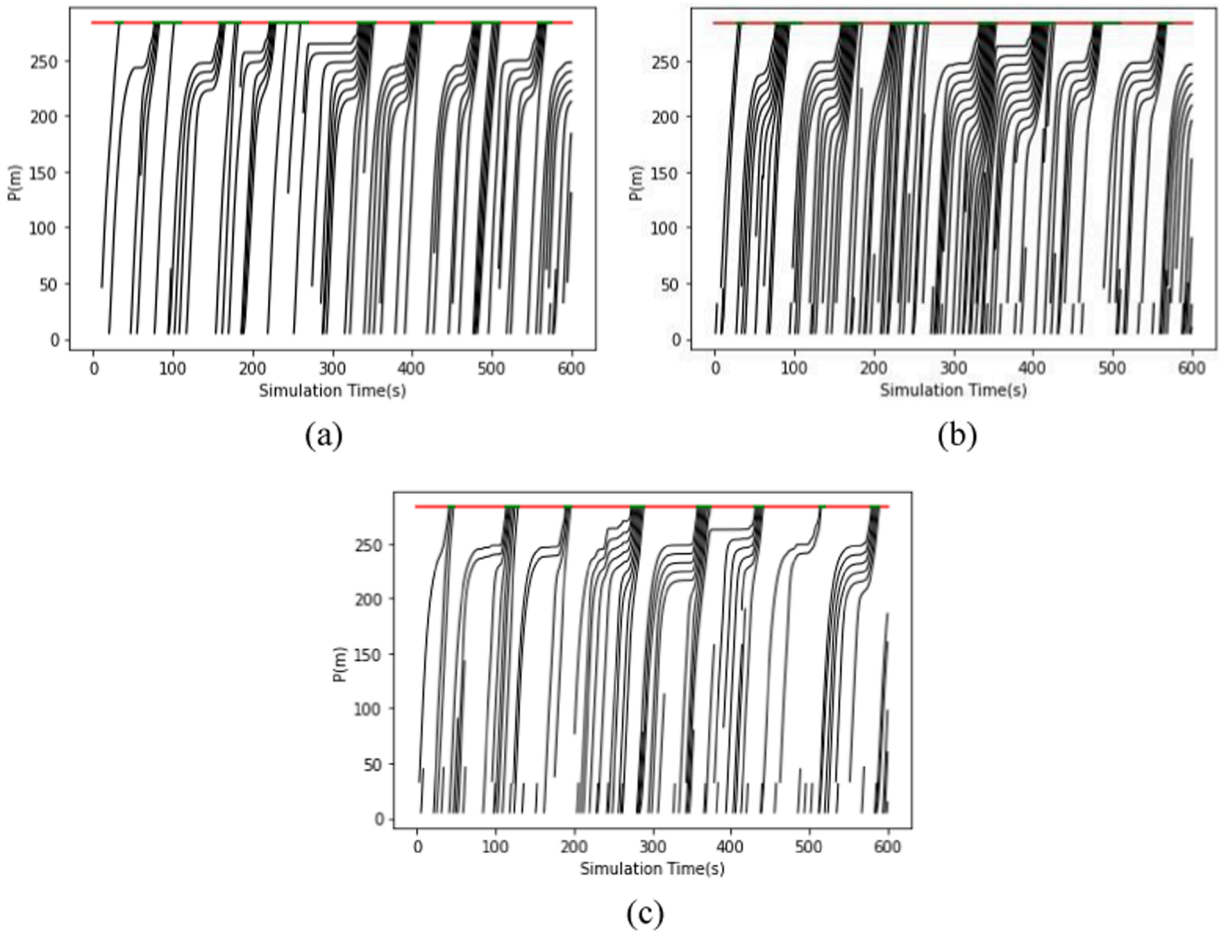

Fig. 9. Trajectories of vehicles in (a) through and right turning lane, (b) through lane (c) left turning only lane. (100% CAV penetration rate, westbound).

$$FDE = \sqrt{(x_N^g - x_N^o)^2 + (y_N^g - y_N^o)^2} \tag{77}$$

Table 4 shows the ADE and FDE for the SUMO dataset, including both car-following and lane changing scenarios. The results indicate that the model performs well in both car-following and lane changing scenarios. Even though the desired time headway for car-following trajectories varies from 1.6 s to 2.0 s, the longitudinal ADE for car-following trajectory is 0.9 m, less than 1/5 of a vehicle length. Although the ADE for the lane change scenario is a little higher (1.68 m), the FDE is only 0.12 m, indicating that the vehicle can reach the desired position precisely at the end of the planning horizon. The result also indicates that the proposed trajectory planning model can mimic lateral driving behavior well. Given that the lane width of the SUMO network is 3.2 m, the lateral ADE (0.27 m) is only 1/12 of the lane width.

4.2. Integrated optimization result analysis

Comprehensive simulation experiments are conducted under different penetration rates and traffic demand levels. Figs. 9-10 show examples of the vehicle trajectories and signal timing of westbound and eastbound directions under 100 % CAV penetration rate. The discontinuous trajectories are caused by lane changes. As shown in Figs. 9-10, CAVs adjust their speeds and lane allocations to pass

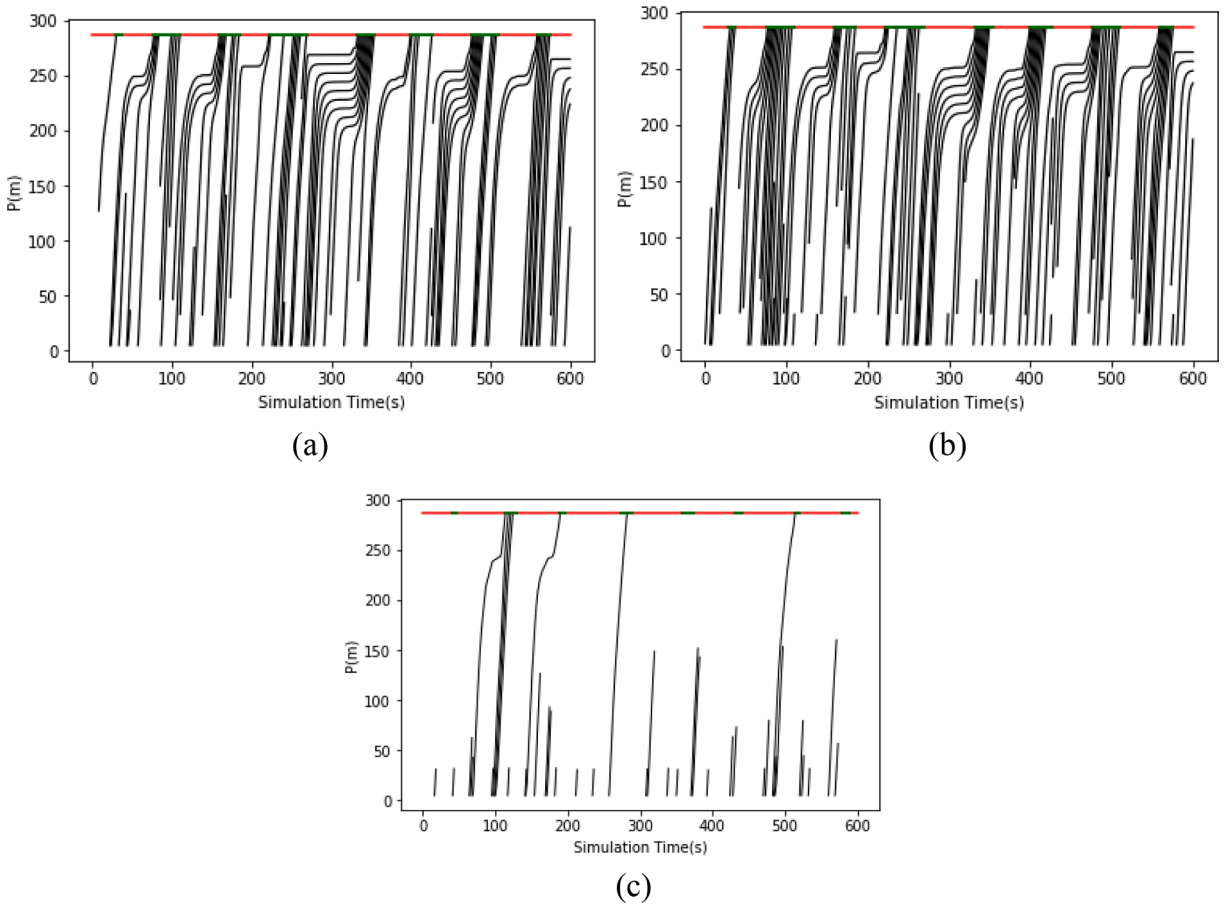

Fig. 10. Trajectories of vehicles in (a) through and right turning lane, (b) through lane (c) left turning only lane. (100% CAV penetration rate, eastbound).

through the intersection during the green time with desired speeds. Most of the CAVs do not need to make complete stops. In some cases, vehicles entering the intersection at the end of the current green phase are assigned a large arrival time and have to stop and wait for the next cycle. The traffic signal adjusts the green durations according to the number of approaching vehicles dynamically. Due to the imbalance traffic volume, although no vehicle is approaching the stop bar at the end of the second cycle in the westbound (Fig. 9**b**), green time is still extended for the approaching vehicles from the eastbound direction (Fig. 10**b**). Figs. 11-12 show an example of vehicle trajectories and signal timing of westbound and eastbound directions under 50 % CAV penetration rate. Compared with Figs. 9-10, the vehicle distribution on the two through lanes is less even and more vehicles have to make complete stops at the intersection. Such differences lead to higher delays and fuel consumption, which will be discussed in the following section.

Fig. 13 and Table 5 show the comparison of average vehicle delay under different scenarios. Note that the "3400 veh/h" scenario represents the real-world traffic demand. The proposed model outperforms the two baselines under all CAV penetration rates and traffic demand levels. The average vehicle delay under 100 % CAV penetration rate when the volume is 3000 veh/h is 27.16 s, 32.63 s when the volume is 3400 veh/h, and 38.60 s when the volume is 3800 veh/h. Compared with the adaptive control, the proposed model reduces the delay by 43.79 %, 49.72 %, and 54.82 % respectively. The delay reduction is mainly due to the reallocation of vehicle arrival time and lanes to balance queues (better utilization of lane capacity) and reduce the startup and clearance delay during the transition period. Compared with the fixed time control, the proposed model can reduce vehicle delays by 54.74 %, 60.12 %, and 63.06 % respectively. Apart from the above-mentioned benefits, compared to fixed-time control, the proposed model dynamically adjusts signal timing according to the number of vehicles approaching the intersection and avoids vehicles stopping twice at the intersection. Note that we set the mean desired headway of CAVs and OVs to be the same in the experiments. The performance can be further improved by considering CAV platooning as in other studies (Yang et al., 2021 Mar).

When the volume grows from 3000 veh/h to 3800 veh/h, the average vehicle delay under 100 % CAV penetration rate only increases slightly from 27.16 s to 38.6 s (11.44 s). Under the adaptive signal control, the vehicle delay increases from 48.32 s to 85.44 s (37.12 s) while under the fixed time control, the vehicle delay increases from 60.01 s to 104.48 s (44.47 s). This comparison illustrates that the proposed model results in higher intersection capacity and is more robust to handle near-saturation and over-saturation traffic conditions.

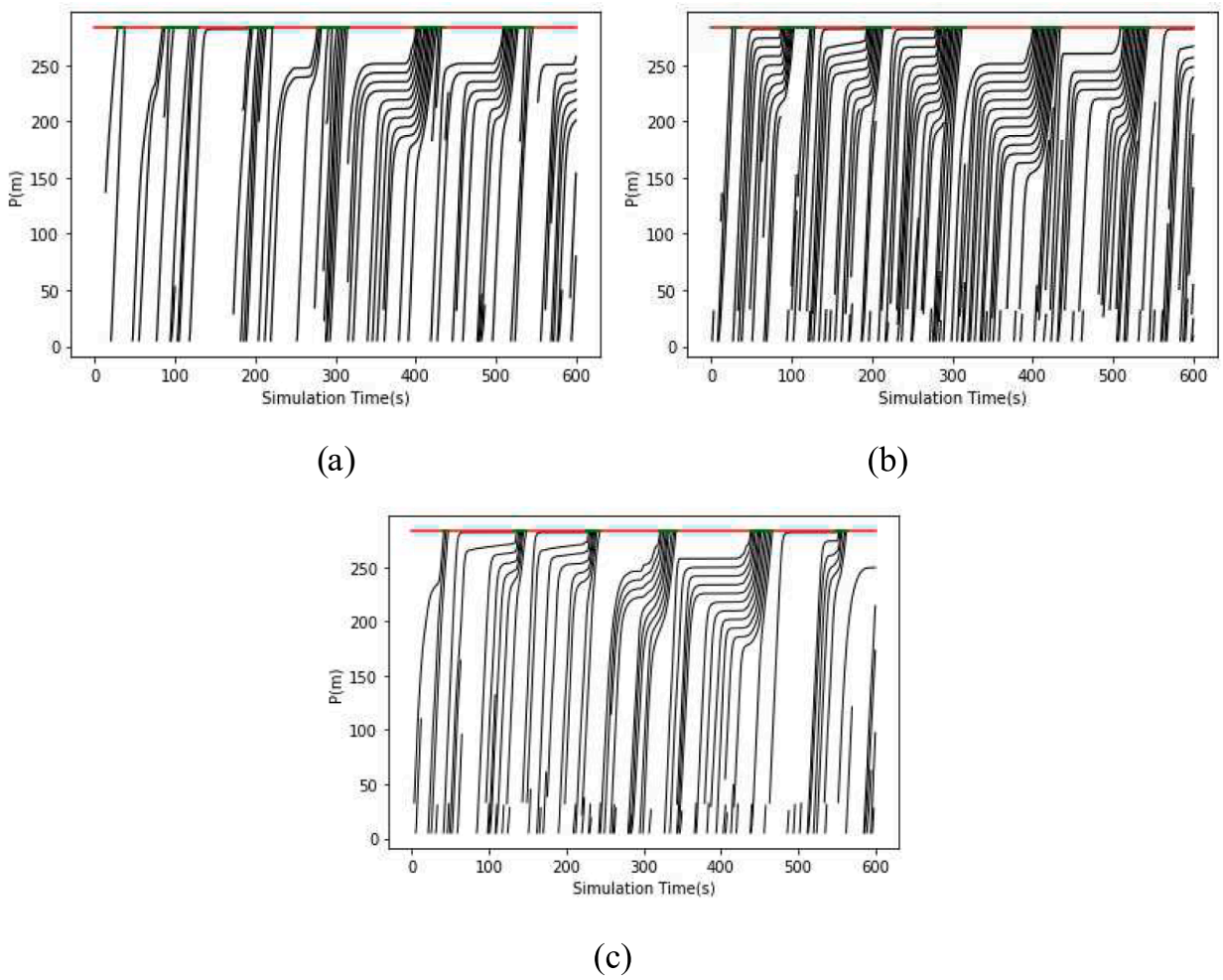

Fig. 11. Trajectories of vehicles in (a) through and right turning lane, (b) through lane (c) left turning only lane. (50% CAV penetration rate, westbound).

When the penetration rate of CAV decreases, the vehicle delay increases under all demand levels. One reason is that OVs need to make complete stops at the red light and introduce startup delays at the beginning of the green signal. Another reason is the prediction errors in the OV trajectories. In the lane changing process, CAVs enable cooperative lane changing by considering the leading lane changing vehicle's future trajectory as a reference when generating its own trajectory. The following CAV in the neighboring lane can obtain the leading CAV's lane changing decision and react to it before the CAV crosses the lane boundary. When the following vehicle is an OV, it will only react to the lane changing CAV when it is close enough to the lane boundary. As a result, the lane changing gap for the CAV may not be fulfilled so that the CAV may not be able to change to the assigned lane and return to its original lane during the lane changing process.

We also investigate the environmental benefit of the proposed model in terms of fuel consumption. Fig. 14 and Table 6 show the comparison of average fuel consumption for the proposed model, adaptive signal control, and fixed time signal control under three demand levels. The calculation of fuel consumption follows the Handbook of Emission Factors for Road Transport (HBEFA) criterion (HBEFA - Handbook Emission Factors for Road Transport [Internet]. [cited, 2023).

The overall trend for fuel consumption is similar to vehicle delays. The proposed model performs better than the adaptive control and fixed time signal control under all CAV penetration rates. The average fuel consumption under 100 % CAV when the volume is 3000 veh/h is 58.96 mg/m and 87.65 mg/m when the volume is 3800 veh/h. There is no significant growth for the proposed model under 100 % CAV when the volume increases. However, the average fuel consumption increases dramatically under adaptive signal control (193.42 mg/m to 556.31 mg/m) and fixed time control (279.27 mg/m to 1225.37 mg/m). Compared with the adaptive control, the proposed model adjusts CAVs' speeds and avoids complete stops at the intersection, reducing fuel consumption during the stop-and-start process. Compared with the fixed time control, the signal timing is adjusted dynamically according to vehicle numbers at each cycle and vehicle distribution among different lanes, effectively avoiding oversaturation (vehicles stop more than once) at the intersection. When the volume is 3800 veh/h, the fuel consumption for 100 % CAV is 87.65 mg/m while for fixed time control is

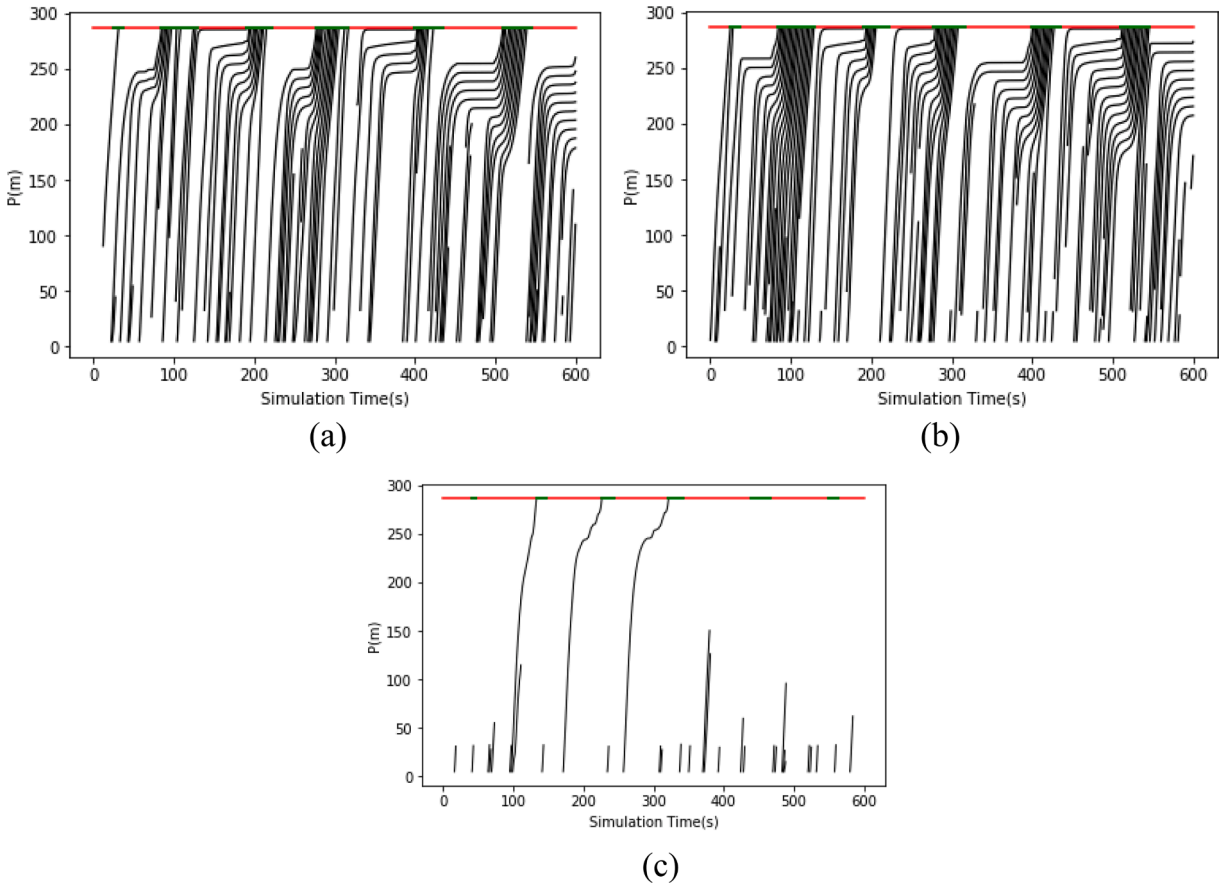

Fig. 12. Trajectories of vehicles in (a) through and right turning lane, (b) through lane (c) left turning only lane. (50% CAV penetration rate, eastbound).

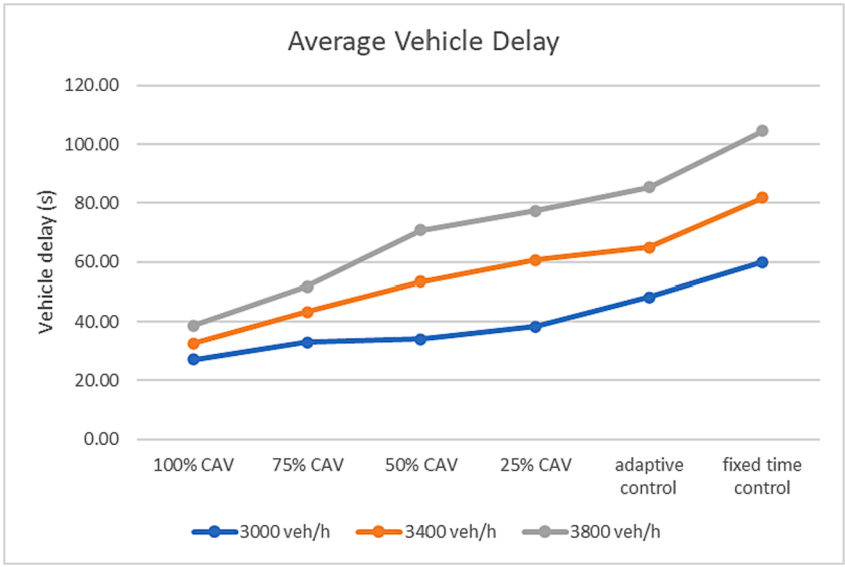

Fig. 13. Average vehicle delay.

Table 5
Average vehicle delay.

Volume	Average delay (s/veh)					
	Proposed control with different penetration rate					
	100 % CAV	75 % CAV	50 % CAV	25 % CAV	Adaptive control	Fixed time control
3000 veh/h	27.16	32.97	34.10	38.30	48.32	60.01
3400 veh/h	32.63	43.33	53.40	60.60	64.90	81.82
3800 veh/h	38.60	51.84	70.82	77.30	85.44	104.48

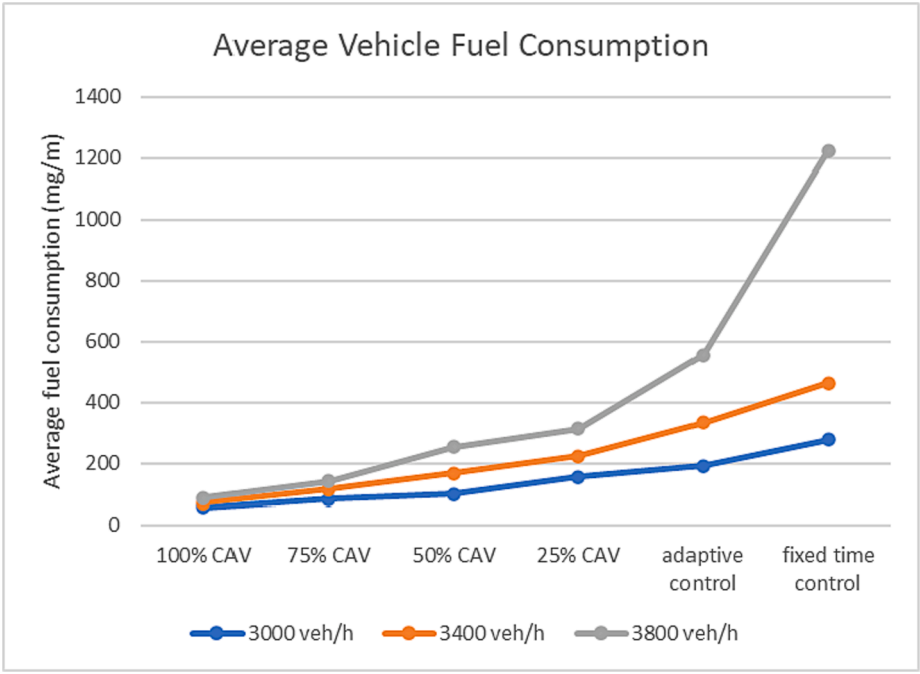

Fig. 14. Average fuel consumption.

Table 6
Average Fuel consumption.

Volume	Average fuel consumption (mg/m)					
	Proposed control with different penetration rate					
	100 % CAV	75 % CAV	50 % CAV	25 % CAV	Adaptive control	Fixed time control
3000 veh/h	58.96	84.91	101.21	155.63	193.42	279.27
3400 veh/h	72.51	116.05	168.62	224.53	333.63	464.05
3800 veh/h	87.65	141.69	254.71	314.95	556.31	1225.37

1225.37 mg/m. Apart from the above-mentioned reasons, when the intersection is over-saturated, some vehicles need to decelerate to change lanes and finish their routes. The slow-moving lane changing vehicles block the following vehicles and increase fuel consumption. However, for 100 % CAV penetration rate, CAVs cooperate to create gaps for neighboring vehicles to change lanes and avoid large deceleration during the lane change process.

5. Conclusions and future research

In this paper, we developed a two-level optimization framework to jointly optimize traffic signal parameters and CAV trajectories under mixed traffic conditions. Different from previous studies, the proposed framework considers a full CAV trajectory planning model, which generates integrated car-following and lane-changing maneuvers. At the high-level, the intersection optimizes the signal timing, CAV arrival time, and arrival lane to minimize the total vehicle delay. At the low-level, each CAV generates detailed trajectories following the guidance from the intersection. Simulation results show that the proposed model can reduce the average vehicle delay by

up to 54.82 % compared with the adaptive signal control and up to 63.06 % compared with the fixed time signal control. Significant fuel consumption benefits are also observed in the simulation experiments.

A few research directions can be pursued in the future. Currently, we conduct the CAV trajectory planning in sequence based on their locations at the intersection. When the traffic volume increases, it becomes more difficult to find a safety gap for CAVs upstream to change lanes thus reducing the solution quality. Multi-agent reinforcement learning can be applied to learn the interaction between vehicles to jointly optimize trajectories for a group of vehicles simultaneously and potentially increase lane change opportunities. In addition, the computation time is quite long (around 1 s) when generating detailed CAV trajectories with a long planning horizon. This is also the main reason why we applied a mid-level reference point generation and split the entire trajectory into smaller segments. A more efficient solution algorithm needs to be developed for solving the high-dimensional nonlinear trajectory generation problem. Finally, extending the current control framework to the network level and considering the route choice behavior is another interesting research direction.

Declaration of competing interest

The authors declare that they have no known competing financial interests or personal relationships that could have appeared to influence the work reported in this paper.

Acknowledgement

This research is supported in part by the U.S. National Science Foundation (NSF) through Grant CPS #2038215. The views presented in this paper are those of the authors alone.

Author contribution statement.

The authors confirm contribution to the paper as follows: study conception and design: Ying, Feng; data collection: Ying; analysis and interpretation of results: Ying, Feng; manuscript preparation: Ying, Feng. Both authors reviewed the results and approved the final version of the manuscript.

References

Anderson SJ, Karumanchi SB, Iagnemma K. Constraint-based planning and control for safe, semi-autonomous operation of vehicles. In: 2012 IEEE Intelligent Vehicles Symposium. 2012. p. 383–8.

Broggi, A., Medici, P., Zani, P., Coati, A., Panciroli, M., 2012. Autonomous vehicles control in the VisLab intercontinental autonomous challenge. Annu Rev Control 36 (1), 161–171.

Car-Following-Models - SUMO Documentation [Internet]. [cited 2023 Mar 11]. Available from: https://sumo.dlr.de/docs/Car-Following-Models.html.

Definition of Vehicles, Vehicle Types, and Routes - SUMO Documentation [Internet]. [cited 2023 Mar 7]. Available from: https://sumo.dlr.de/docs/Definition_of_Vehicles%2C_Vehicle_Types%2C_and_Routes.html.

Elbanhawi, M., Simic, M., 2014. Sampling-based robot motion planning: A review. IEEE Access 2, 56–77.

Feng, Y., Yu, C., Liu, H.X., 2018. Spatiotemporal intersection control in a connected and automated vehicle environment. Transportation Research Part c: Emerging Technologies. 1 (89), 364–383.

Ferguson, D., Howard, T.M., Likhachev, M., 2008 Nov. Motion planning in urban environments: Ferguson, howard, & likhachev: motion planning in urban environments. J Field Robotics. 25 (11–12), 939–960.

Glaser, S., Vanholme, B., Mammar, S., Gruyer, D., Nouvelière, L., 2010. Maneuver-based trajectory planning for highly autonomous vehicles on real road with traffic and driver interaction. IEEE Trans. Intell. Transp. Syst. 11 (3), 589–606.

Gonzalez Bautista, D., Pérez, J., Milanes, V., Nashashibi, F., 2015. A review of motion planning techniques for automated vehicles. IEEE Trans. Intell. Transp. Syst. 26 (17), 1–11.

Gu T, Dolan JM. On-Road Motion Planning for Autonomous Vehicles. In: Su CY, Rakheja S, Liu H, editors. Intelligent Robotics and Applications [Internet]. Berlin, Heidelberg: Springer Berlin Heidelberg; 2012 [cited 2023 Mar 8]. p. 588–97. (Hutchison D, Kanade T, Kittler J, Kleinberg JM, Mattern F, Mitchell JC, et al., editors. Lecture Notes in Computer Science; vol. 7508). Available from: http://link.springer.com/10.1007/978-3-642-33503-7_57.

Guo, Y., Ma, J., Xiong, C., Li, X., Zhou, F., Hao, W., 2019. Joint optimization of vehicle trajectories and intersection controllers with connected automated vehicles: Combined dynamic programming and shooting heuristic approach. Transportation Research Part c: Emerging Technologies. 1 (98), 54–72.

HBEFA - Handbook Emission Factors for Road Transport [Internet]. [cited 2023 Mar 9]. Available from: https://www.hbefa.net/e/index.html.

Islam, S.M.A.B.A., Hajbabaie, A., 2017. Distributed coordinated signal timing optimization in connected transportation networks. Transportation Research Part c: Emerging Technologies. 1 (80), 272–285.

Jeon J hwan, Cowlagi RV, Peters SC, Karaman S, Frazzoli E, Tsiotras P, et al. Optimal motion planning with the half-car dynamical model for autonomous high-speed driving. In: 2013 American Control Conference. 2013. p. 188–93.

Jiang, X., Shang, Q., 2022. A dynamic CAV-dedicated lane allocation method with the joint optimization of signal timing parameters and smooth trajectory in a mixed traffic environment. IEEE Trans. Intell. Transp. Syst. 1–14.

Jiang, Y., Zhao, B., Liu, M., Yao, Z., Li, L., 2021. A two-level model for traffic signal timing and trajectories planning of multiple CAVs in a random environment. J. Adv. Transp. 2021, 1–13.

Kala R, Warwick K. Planning of multiple autonomous vehicles using RRT. In: 2011 IEEE 10th International Conference on Cybernetic Intelligent Systems (CIS). 2011. p. 20–5.

Kala, R., Warwick, K., 2013. Multi-level planning for semi-autonomous vehicles in traffic scenarios based on separation maximization. J. Intell. Rob. Syst. 72 (3-4), 559–590.

Kiran BR, Sobh I, Talpaert V, Mannion P, Sallab AAA, Yogamani S, et al. Deep Reinforcement Learning for Autonomous Driving: A Survey [Internet]. arXiv; 2021 [cited 2022 Jul 31]. Available from: http://arxiv.org/abs/2002.00444.

Kogan, D., & Murray, R. (2006, December). Optimization-based navigation for the DARPA Grand Challenge. In *Conference on Decision and Control (CDC)*.

Kuderer M, Gulati S, Burgard W. Learning driving styles for autonomous vehicles from demonstration. In: 2015 IEEE International Conference on Robotics and Automation (ICRA). 2015. p. 2641–6.

The Leader in Decision Intelligence Technology - Gurobi Optimization [Internet]. [cited 2023 Mar 11]. Available from: https://www.gurobi.com/.

Li, Z., Elefteriadou, L., Ranka, S., 2014. Signal control optimization for automated vehicles at isolated signalized intersections. Transportation Research Part c: Emerging Technologies. 1 (49), 1–18.

Mannering, F.L., Washburn, S.S., 2020. Principles of highway engineering and traffic analysis. John Wiley & Sons, p. 416.

Nallamothu, S., Stark, J., Birriel, E., Inamdar, I., Rosenbohm, N., Shah A., Ticatch, J., Vadakpat G., Detailed Concept of Operations: Transportation Systems Management and Operations/Cooperative Driving Automation Use Cases and Scenarios, December 2020 - FHWA-HRT-20-064 [Internet]. [cited 2022 Jul 31]. Available from: https://www.fhwa.dot.gov/publications/research/operations/20064/index.cfm.

Niroumand, R., Tajalli, M., Hajibabai, L., Hajbabaie, A., 2020. Joint optimization of vehicle-group trajectory and signal timing: Introducing the white phase for mixed-autonomy traffic stream. Transportation Research Part c: Emerging Technologies. 1 (116), 102659.

Pyomo [Internet]. Pyomo. [cited 2023 Mar 11]. Available from: http://www.pyomo.org.

SublaneModel - SUMO Documentation [Internet]. [cited 2023 Mar 11]. Available from: https://sumo.dlr.de/docs/Simulation/SublaneModel.html.

Vorobieva H, Minoiu-Enache N, Glaser S, Mammar S. Geometric continuous-curvature path planning for automatic parallel parking. In: 2013 10th IEEE INTERNATIONAL CONFERENCE ON NETWORKING, SENSING AND CONTROL (ICNSC). 2013. p. 418–23.

Weng B, Rao SJ, Deosthale E, Schnelle S, Barickman F. Model Predictive Instantaneous Safety Metric for Evaluation of Automated Driving Systems. In: 2020 IEEE Intelligent Vehicles Symposium (IV). 2020. p. 1899–906.

Xu, B., Ban, X.J., Bian, Y., Li, W., Wang, J., Li, S.E., Li, K., 2019. Cooperative method of traffic signal optimization and speed control of connected vehicles at isolated intersections. IEEE Trans Intell Transport Syst. 20 (4), 1390–1403.

Yang, Z., Feng, Y., Liu, H.X., 2021. A cooperative driving framework for urban arterials in mixed traffic conditions. Transportation Research Part c: Emerging Technologies. 1 (124), 102918.

Ying, J., Feng, Y., 2022. Full vehicle trajectory planning model for urban traffic control based on imitation learning. Transp. Res. Rec. 2676 (7), 186–198.

Yu, C., Feng, Y., Liu, H.X., Ma, W., Yang, X., 2018. Integrated optimization of traffic signals and vehicle trajectories at isolated urban intersections. Transp. Res. B Methodol. 1 (112), 89–112.

Yu, C., Feng, Y., Liu, H.X., Ma, W., Yang, X., 2019. Corridor level cooperative trajectory optimization with connected and automated vehicles. Transportation Research Part c: Emerging Technologies. 1 (105), 405–421.

Zhang J, Cho K. Query-Efficient Imitation Learning for End-to-End Autonomous Driving. arXiv:160506450 [cs] [Internet]. 2016 May 20 [cited 2021 Jul 30]; Available from: http://arxiv.org/abs/1605.06450.

Zhang S, Deng W, Zhao Q, Sun H, Litkouhi B. Dynamic Trajectory Planning for Vehicle Autonomous Driving. In: 2013 IEEE International Conference on Systems, Man, and Cybernetics. 2013. p. 4161–6.